Journal of Inorganic and Organometallic Polymers and Materials (2024) 34:5831–5853
https://doi.org/10.1007/s10904-024-03189-y

RESEARCH

Biosynthesis of Silver and Gold Nanoparticles Using *Geum urbanum* L. Rhizome Extracts and Their Biological Efficiency

Irina Macovei[1] · Valeria Harabagiu[2] · Ana Flavia Burlec[1] · Cornelia Mircea[1] · Cristina Elena Horhogea[3] · Cristina Mihaela Rimbu[3] · Liviu Săcărescu[2] · Alina-Diana Panainte[1] · Anca Miron[1] · Monica Hăncianu[1] · Constantin Nechita[4] · Andreia Corciova[1]

Received: 29 April 2024 / Accepted: 7 June 2024 / Published online: 15 July 2024
© The Author(s) 2024

Abstract

The present study evaluates the biosynthesis of AgNPs and AuNPs using aqueous and ethanolic *Geum urbanum* L. rhizome extracts. The biosynthesized metal nanoparticles (MNPs) were characterized using UV-Vis spectroscopy, FTIR, DLS, SEM, EDX, and TEM. The UV-Vis spectra confirmed the synthesis of AgNPs and AuNPs through peaks corresponding to the surface plasmon effect of metallic Ag (400–430 nm) and Au (530–570 nm). FTIR analysis indicated that alcohols, phenols, proteins, and carbohydrates from *G. urbanum* rhizome extracts composition are involved in MNPs synthesis. In DLS analysis, AgNPs (34.26–41.14 nm) showed smaller hydrodynamic diameters than AuNPs (46.26–70.29 nm). At the same time, all values for zeta potential were negative, between −21 and −13 mV, suggesting good stabilities for all the colloidal MNPs systems in dispersion. TEM analysis showed that the biosynthesized AgNPs had a spherical morphology, while AuNPs were quasi-spherical, polygonal, and triangular. According to TEM data, AgNPs synthesized using aqueous and ethanolic *G. urbanum* rhizome extracts were characterized by mean diameters of 9.82 ± 3.68 and 14.29 ± 3.46 nm, while AuNPs by 15.88 ± 6.28 and 24.89 ± 10.75 nm, respectively. EDX analysis confirmed the presence of metallic Ag and Au in the MNPs composition by detecting strong signals at 3 (AgNPs) and 2.2 keW (AuNPs). In disc diffusion assay, MNPs showed good antimicrobial activity against Gram-positive (*S. aureus* MSSA, *S. aureus* MRSA, *S. epidermidis*) and Gram-negative (*E. coli, P. aeruginosa, K. pneumoniae*) bacteria and yeasts (*C. albicans*). AgNPs and AuNPs were also characterized by a significant antioxidant potential, evaluated through in vitro assays (lipoxygenase inhibition, DPPH radical scavenging activity, metal ion chelating activity, and hydroxyl radical scavenging assays). An overall better activity was obtained for the ethanolic *G. urbanum* rhizome extract and its derived AgNPs (EC_{50} = 34.2 ± 1.86 mg/mL in lipoxygenase inhibition assay). Therefore, the *G. urbanum* rhizome extracts proved to be excellent sources for biologically active AgNPs and AuNPs.

Keywords Green synthesis · Noble metal nanoparticles · Physicochemical characterization · Antimicrobial activity · Antioxidant activity

✉ Valeria Harabagiu
hvaleria@icmpp.ro

✉ Constantin Nechita
constantin.nechita@icas.ro

[1] Grigore T. Popa University of Medicine and Pharmacy, Faculty of Pharmacy, Iasi 700115, Romania

[2] Petru Poni Institute of Macromolecular Chemistry, Iasi 700487, Romania

[3] Department of Public Health, University of Life Sciences Ion Ionescu de la Brad, Iasi 700489, Romania

[4] National Institute for Research and Development in Forestry 'Marin Dracea', Câmpulung Moldovenesc 725100, Romania

1 Introduction

The increased pathogenic microorganisms' resistance to chemically synthesized antibiotics is of global concern and has induced a vast interest in finding natural alternatives [1, 2]. Antimicrobial resistance is a worldwide problem, and several leading pathogens are associated with resistance to synthetic drugs, including *Escherichia coli*, *Staphylococcus aureus*, *Pseudomonas aeruginosa*, and *Klebsiella pneumoniae*, causing several millions of deaths yearly [3]. The costs for treatment of those invasive infections are impressive, only in the US for community and hospital-onset

overhead of $ 4.6 billion, indicating the magnitude of both health and economic losses [4]. The noble metal nanoparticles (MNPs) can fight these infections through various mechanisms, penetrating the bacteria cell wall and causing several dysfunctions due to their small size and irregular shape [1, 5, 6]. Many scientific reports show the remarkable toxicity of silver nanoparticles (AgNPs) against Gram-positive and Gram-negative bacteria and yeasts, underlying an improved activity for the plant-mediated synthesized ones [7, 8]. Due to their significant antimicrobial activity, AgNPs are already included in drug delivery vectors, dental products, and surgical tools [9–11]. The anticancer activity of plant-mediated synthesized MNPs was also demonstrated in recent studies [12, 13]. The phyto-functionalized AgNPs and gold nanoparticles (AuNPs) showed various biological activities, as is the case of those prepared with an aqueous *Euphrasia officinalis* L. leaf extract when AgNPs inhibited human lung cancer (A549) and cervical cancer (HeLa) cell lines. At the same time, AuNPs were active only against cervical cancer cell lines [14]. AgNPs synthesized with *Rotheca serrata* L. Steane & Mabb. flower bud extract demonstrated efficiency against pancreatic ductal adenocarcinoma cells [13]. Similar results illustrate that AgNPs biosynthesized from *Cardamine hirsute* L. leaf extract acted efficiently against Caco-2 colorectal adenocarcinoma cell line [15]. AgNPs biosynthesized using *Cucumis sativus* var. hardwickii fruit extract possessed a significant cytotoxic effect against human ovarian teratocarcinoma (Pa-1) [16]. The biological activities of MNPs depend on their chemical and physical properties (size, shape, surface functionalization) [11]. A recent study found that larger particles showed significantly increased toxicity against pathogenic microorganisms and mammalian cells, contradicting previous considerations based on which smaller dimensions are better for the biological potential [17]. For AuNPs, the mechanisms proposed for the antibacterial activity rely on the deterioration of the microorganisms' cell wall and membrane or inhibition of the binding ribosome tRNA [18, 19]. A more complex process is associated with AgNPs toxicity against bacteria, which is considered to be related to the destruction of cell walls and plasma membranes [20], induction of ROS production in the cytoplasm [21], and alteration of protein synthesis [22].

Noble metal nanoparticles have received valuable interest in pharmaceutical and medical studies due to their chemical, physical, and biological characteristics [23]. The synthesis of biofunctionalized MNPs using plant extracts is eco-friendly, biocompatible, cost-efficient, clean, and less hazardous [24]. Plant extracts composition in secondary metabolites is associated with valuable biological activities, e.g., antioxidant, antidiabetic, antibacterial, antiviral, or anticancer properties [25, 26]. The phenolic compounds, flavonoids, tannins, anthocyanins, and alkaloids in leaves, barks, roots, stems, seeds, and fruit extracts were investigated for their potential in MNPs production, including AgNPs and AuNPs. Moreover, during the synthesis, several phytochemicals attach to the MNPs surface, stabilizing and modulating the biological activities due to their antibacterial, antioxidant, and anticancer intrinsic activities [27–29]. A large number of plant extracts were used for AgNPs and AuNPs synthesis, such as *Indigofera tinctoria* L. aqueous leaf extract [30, 31], *Phyllanthus emblica* L. ethanolic fruit extract [32], *Rumex roseus* L. methanolic whole plant extract [33], *Curcuma longa* L. aqueous rhizome extract [34], or *Cibotium barometz* (L.) J. Sm. aqueous root extract [35]. Other reports show the MNPs synthesis with various plant extracts, covering species from more than one plant family, e.g., Phyllanthaceae, Lamiaceae, Rutaceae, and Euphorbiaceae [36]. The authors show that the plant extract phytochemicals used in MNPs synthesis are responsible for their remarkable biological activities, including cytotoxic, anticancer, antidiabetic, and antibacterial properties. Furthermore, scientific reports show that *Ricinus communis* L. ethanolic leaf extract-mediated AuNPs possess significant potential to inhibit hepatocellular carcinoma (HepG2) cell lines [37]. However, the study also found that while the *R. communis* ethanolic leaf extract was safe, the derived phyto-functionalized AuNPs showed hemolytic activity, harming red blood cells. Such results require a careful evaluation, and further in-depth analysis must be conducted to guarantee the safe use of biofunctionalized MNPs.

Geum urbanum L. is used in traditional medicine for stomach ulcers, febrile disease, digestive disorders, hemorrhoids, and intestinal tract irritations [38]. Roots and rhizomes contain high amounts of phenylpropanoids (eugenol and tannins), dehydrodigallic acid, phenolic derivates, eugenol, gallo- and ellagitannins (pedunculagin, stachyurin, casuarynin, and gemin), procyanidins, and steroids, often found in many species of the Rosaceae family [39, 40]. *G. urbanum* can increase the expression of several essential cardiogenic markers, α-actinin, and cardiac troponin [41]. An *G. urbanum* aqueous rhizome extract having an ellagitannin (gemin A) as the main constituent was found to be effective in treating cavity inflammation disorders, such as mucositis, gingivitis, and periodontosis [42]. The authors suggest that gemin A is mainly responsible for the anti-inflammatory activity by altering the neutrophil cells' functions by inhibiting reactive oxygen species, proteases, chemokines, cytokines release, and stimulation of TNF-alfa expression. *Geum* species rhizomes and aerial organs contain ellagic, linoleic, palmitic, and stearic acids [43], which showed anti-inflammatory, antioxidant, neuroprotective, hypotensive, antineoplastic, antidiabetic, and antimicrobial activities [42, 44–46]. Even so, the *G. urbanum* rhizome extract potential

for MNPs biosynthesis has scarcely been investigated until the present, as there is only one study on the Web of Science database that previously evaluated the phytotoxicity of bimetallic Ag/Au nanoparticles synthesized using *G. urbanum* aqueous extract [47]. Thus, our study aimed to bio-synthesize AgNPs and AuNPs in an optimized manner using *G. urbanum* aqueous and ethanolic rhizome extracts followed by physicochemical characterization. Further, comparative biological testing (antimicrobial and antioxidant activities) was conducted for AgNPs and AuNPs phyto-functionalized with aqueous and ethanolic *G. urbanum* rhizome extracts against several pathogens.

2 Materials and methods

2.1 Chemical and Reagents

Follin-Ciocalteu's phenol reagent, gallic acid, sodium carbonate, silver nitrate ($AgNO_3$), chloroauric acid ($HAuCl_4$), dimethyl sulfoxide (DMSO), linoleic acid, soybean 15-lipoxygenase, 2,2-diphenyl-1-picryl-hydrazyl (DPPH), sodium acetate, ferrozine, hydrogen peroxide, and sodium salicylate were purchased from Sigma-Aldrich (Steinheim, Germany). Absolute ethanol and methanol were supplied by Chimreactiv (Bucharest, Romania). Hydrochloric acid 37%, sodium hydroxide, and ferrous sulfate heptahydrate were obtained from Merck (Darmstadt, Germany). Mueller-Hinton agar, gentamicin (10 µg/disk), and nystatin (100 units/disk) were provided by Oxoid (Basingstoke, UK). Potato dextrose agar came from Bio-Rad (Hercules, CA, USA). Ultrapure water was obtained from the SG Water Ultra Clear TWF water purification system (Barsbüttel, Germany).

2.2 Microorganisms

Staphylococcus aureus ATCC 25,293 and ATCC 43,300, *Staphylococcus epidermidis* ATCC 12,228, *Escherichia coli* ATCC 25,922, *Pseudomonas aeruginosa* ATCC 9027, *Klebsiella pneumoniae* ATCC 13,883 and *Candida albicans* ATCC 90,028 were purchased from the American Type Culture Collection (ATCC, Manassas, VA, USA).

2.3 Preparation of *G. urbanum* Rhizome Extracts

Grounded *G. urbanum* rhizomes (purchased from a local natural products store) were subjected to extraction in a ratio of 1:10 using ultra-pure water and ethanol (70%), following a procedure previously described [48]. The plant material was mixed with the solvent and maintained under magnetic stirring (400 rpm) for 3 h, followed by filtration. The extracts were stored at -20 °C until further use.

2.4 Chemical Characterization of *G. urbanum* Rhizome Extracts

The total phenolic content of aqueous and ethanolic rhizome extracts was assessed by the Folin-Ciocalteu method, as previously described [49]. In brief, the absorbance of the reaction mixture (0.04 mL sample, 3.16 mL ultra-pure water, 0.2 mL Folin-Ciocalteu reagent, and 0.6 mL 20% sodium carbonate solution) was determined at 765 nm after 2 h incubation at room temperature (Specord 210 Plus spectrophotometer, Analytik Jena, Jena, Thuringia, Germany). The phenolic content was expressed as gallic acid equivalents (mg/mL). The assay was carried out in triplicate and expressed as mean ± standard deviation.

2.5 Optimized Synthesis of AgNPs and AuNPs

The noble metal nanoparticle synthesis was monitored and optimized by recording the UV-Vis spectra of the reaction mixtures in the wavelength of 350–600 nm (AgNPs) and 400–700 nm (AuNPs) [48, 50, 51], respectively, on a Specord 210 Plus spectrophotometer (Analytik Jena, Thuringia, Germany). Several experiments were conducted to obtain the maximum yield of AgNPs and AuNPs by testing different values for parameters such as $AgNO_3$ and $HAuCl_4$ concentrations (1, 2, 3 and 5 Mm and 1, 3 and 5 mM, respectively), pH (4, 6, 8 and 10) adjusted with HCl 0.1 M and NaOH 0.1 M solutions, ratios of rhizome extract and $AgNO_3$ or $HAuCl_4$ (1:9, 5:5, and 9:1), temperature (20, 40, and 70 °C) and reaction time (10, 20, 30, 40, 50, 60, 90, 120, and 180 min). MNPs synthesis was further conducted using the optimal conditions achieved through optimization studies. The colloidal MNPs dispersions obtained were centrifuged at 6800 rpm for 30 min (Hettich Rotina 380 R centrifuge, Hettich, Tuttlingen, Germany), and the resulting sediment was washed two times with ulta-pure water to eliminate unreacted substances. Solid MNPs pellets were finally obtained by freeze-drying (Unicryo TFD 5505 freeze dryer, UniEquip GmbH, Munich, Germany) and stored at -4 °C until further use.

2.6 Characterization of AgNPs and AuNPs

AgNPs and AuNPs characterization were achieved by using attenuated total reflection Fourier-transform infrared (ATR-FTIR) spectroscopy, dynamic light scattering (DLS), scanning electron microscopy (SEM), energy dispersive X-ray analysis (EDX) and transmission electron microscopy (TEM). The procedures were implemented as previously described [48] with minor changes. ATR-FTIR spectroscopy was used to identify the functional groups and compounds from the rhizome extracts that acted as reducing and

capping agents in MNPs synthesis [52]. Briefly, a volume (30 mL) of aqueous and ethanolic rhizome extract was concentrated under reduced pressure at 40 °C (Büchi R–210 rotary evaporator system, Büchi Labortechnik AG, Flawil, Switzerland) and freeze-dried (Unicryo TFD 5505 freeze dryer, UniEquip GmbH, Munich, Germany). Freeze-dried MNPs and rhizome extracts were subjected to ATR-FTIR measurements (Bruker Alpha-P ATR FTIR spectrometer, Bruker, Ettlingen, Germany), with a resolution of 4 cm^{-1} in the spectral region of 4000–400 cm^{-1}. Spectral data were processed using Bruker OPUS spectroscopy software ver. 7 ed. 2011. DLS measurements made on a Malvern Zetasizer Nano-ZS (Malvern Instruments, Malvern, UK) revealed the hydrodynamic diameters (D_H), polydispersity index (PDI), and zeta potential values for the colloidal MNPs dispersions. A red He/Ne laser (633 nm) was used for D_H evaluation, and zeta potential was recorded using electrophoretic light scattering [53]. The morphology, size, and chemical composition of AgNPs and AuNPs were achieved through SEM coupled with EDX [54] and TEM [55]. MNPs pellets were operated in low vacuum mode at 20 kV using a Quanta 200 scanning electron microscope with an energy dispersive spectrometer (FEI Company, Hillsboro, OR, USA). Before TEM analysis, a drop of each colloidal MNPs dispersion was placed on a 300-mesh carbon-coated copper grid (Ted Pella) and vacuum-dried for 24 h (room temperature). Samples were investigated in high contrast mode at 120 kV accelerating voltage on a Hitachi High-Tech HT7700 transmission electron microscope (Hitachi High-Technologies Corporation, Tokyo, Japan). TEM images were also used to assess particle sizes by the use of image-J software [55].

2.7 Biological Activities of AgNPs and AuNPs

2.7.1 Antimicrobial Activity

Disk diffusion assay was performed to investigate the antibacterial activity of AgNPs and AuNPs against Gram-positive (*S. aureus, S. epidermidis*) and Gram-negative (*E. coli, P. aeruginosa, K. pneumoniae*) bacteria and yeasts (*C. albicans*). Cell suspensions corresponding to 0.5 McFarland turbidity standard (equivalent to 1.5 × 10^6 colony forming units (CFU)/mL) were prepared from the pure and fresh microbial cultures (24 h) and adjusted using the Biosan DEN-1B densitometer (Biosan, Riga, Latvia). The surface of the culture media for bacteria (Mueller-Hinton Agar) and for yeasts (Potato Dextrose Agar) was flooded with 1 mL of microbial suspension, and the excess was removed using a Pasteur pipette. Sterile filter paper discs (diameter 5 mm) loaded with 30 µL MNPs were spread on the surface of the culture media for bacteria and yeasts and then incubated under the same aerobic conditions for 24 h at 37 °C. The diameters of the inhibition zones were then measured [48, 56]. Gentamicin (10 µg/disk) and nystatin (100 units/disk) were positive controls.

2.7.2 In Vitro Lipoxygenase Inhibition (LOX) Assay

The extracts and their derived MNPs were evaluated for their lipoxygenase inhibitory potential using LOX enzyme and linoleic acid as the substrate. 0.05 mL of soybean 15–lipoxygenase solution) borate buffer pH 9 was mixed with 0.05 mL of sample solution diluted in dimethylsulfoxide (DMSO) and incubated for 10 min at room temperature. Further, 2 mL solution of 0.16 M linoleic acid in 0.1 M borate buffer pH 9 was added. The absorbance of the mixture was recorded at 234 nm in the time interval of 0–120 s. In parallel, the positive control was assessed by replacing the sample volume with DMSO. The percentage of LOX inhibitory activity was determined using Eq. 1.

$$LOX\ inhibitory\ activity\,(\%) = \frac{A_{EFI} - A_{ECI}}{A_{EFI}} \times 100 \qquad (1)$$

where, A_{EFI} represents the difference between the absorbance of the enzyme solution without inhibitor at 90 s and the absorbance of the same solution at 30 s; A_{ECI} is the difference between the absorbance of the enzyme solution treated with an inhibitor (sample) at 90 s and the absorbance of the same solution at 30 s. For the samples in which a lipoxygenase inhibition capacity of more than 50% was obtained, the half-maximal effective concentration (EC_{50}) was calculated. The concentration of the antioxidant agent solution corresponding to an activity of 50% (EC_{50}) was obtained by linear interpolation, taking into account the first lower value below 50% and, respectively, the first higher value above 50%.

2.7.3 DPPH Radical Scavenging Activity

DPPH radical scavenging activity of aqueous and ethanolic *G. urbanum* rhizome extracts and their derived AgNPs and AuNPs was also evaluated. Briefly, 0.3 mL sample solution in DMSO was mixed with 2.7 mL DPPH methanolic solution (4 mg %). The prepared solution was incubated for 10 min at room temperature and dark, followed by recording the absorbance at 517 nm. Control was prepared in the same conditions, but the sample volume was replaced with DMSO. The percentage of DPPH inhibitory activity was evaluated according to Eq. 2:

$$DPPH\ inhibitory\ activity\,(\%) = \frac{A_C - A_S}{A_C} \times 100 \qquad (2)$$

where, A_c represents the absorbance of the control; A_s is the absorbance of the sample.

EC_{50} values were calculated as described in 2.7.2.

2.7.4 Metal Ion Chelating Activity Assay

To evaluate the Fe^{2+} chelation capacity for the aqueous and ethanolic *G. urbanum* rhizome extracts and their derived AgNPs and AuNPs, it was performed a protocol based on the formation of a pink complex between ferrozine and Fe^{2+} with an absorbance maximum at 562 nm. An aliquot of 0.2 mL of sample solution in ultrapure water was added to 0.74 mL of 0.1 M acetate buffer solution (pH 5.25) and 0.02 mL of 2 mM ferrous sulfate solution in 0.2 M hydrochloric acid, followed by shaking for 10–15 s. Then, 0.04 mL of 5 mM ferrozine solution was added to the above mixture and incubated for 10 min in a dark environment. Absorbance was recorded at 562 nm, using the same mixture as blank, except for the ferrous sulfate solution, which was replaced with ultrapure water. In parallel, the control was prepared by replacing the sample volume with ultrapure water. The Fe^{2+} chelating activity was calculated using Eq. 3 [57, 58]:

$$Activity\,(\%) = \frac{A_C - A_S}{A_C} \times 100 \tag{3}$$

where, A_c represents the absorbance of the control; A_s is the absorbance of the sample. EC_{50} values were calculated as described in 2.7.2.

2.7.5 Hydroxyl Radical Scavenging Assay

The hydroxyl radical was quantified spectrophotometrically based on the hydroxylation of salicylic acid by the hydroxyl radical (released through the reaction between Fe^{2+} and hydrogen peroxide) with a resulting violet-pink complex with a maximum absorbance at 562 nm [59]. The aqueous and ethanolic *G. urbanum* rhizome extracts and their derived AgNPs and AuNPs were samples analyzed. Briefly, 0.225 mL of the sample solution in DMSO was mixed with 0.750 mL of 1.5 mM ferrous sulfate, 0.9 mL of 20 mM sodium salicylate solution, and 0.525 mL of 6 mM hydrogen peroxide solution. The mixture was incubated for 30 min at 37 °C. After cooling to room temperature, the absorbance of the sample (control) was read at 562 nm with a blank for which the ferrous sulfate solution was replaced with ultrapure water. Control was processed under the same conditions as the samples by replacing the volume of the sample with DMSO. The hydroxyl radical scavenger activity was calculated using Eq. 3; EC_{50} values were calculated as described at 2.7.2.

2.8 Statistical Analysis

Each experiment was performed in triplicate, and the experimental results were assessed for statistical significance using the Student's *t*-test ($p \leq 0.05$). Summary statistics were presented, including mean (σ) and standard deviation (sd). One-way analysis of variance (ANOVA) was performed to evaluate the statistically significant differences between samples at $p < 0.05$. D'Agostino K-Squared and Shapiro-Wilk normality tests to evaluate nanoparticle size distribution from the four datasets. The statistical analysis was computed using SPSS software v27.

3 Results and Discussions

3.1 Phenolic Content of Rhizome Extracts

In this study, AgNPs and AuNPs were green-synthesized using two *G. urbanum* rhizome extracts (aqueous and ethanolic). When mixed with a metal salt ($AgNO_3$/$HAuCl_4$), phytochemicals from the plant extract act as reducing agents, providing metallic Ag and Au. Moreover, other biomolecules attach to the metal nanoparticle surface, assuring the system's stability and acting as capping agents. These capping agents are further responsible for modulating the specificity and intensity of the biological activities of MNPs. As already stated in previous reports, among plant phytochemicals, phenols are mainly responsible for the reduction and stabilization involved in MNPs synthesis [60, 61]. The reducing capacity of phenolic compounds relies on the oxidative of hydroxyl groups (R–OH) to carbonyl groups (R–C = O) [62]. *G. urbanum* rhizomes represent an essential source of phenylpropanoids, especially eugenol and tannins, known for their analgesic, antimicrobial, anti-inflammatory, and antioxidant activities [63, 64]. However, the composition of extracts is critically influenced by the solvent used for extraction due to phytochemicals' different solubility [38]. Therefore, the present study's first objective was to quantify the total phenolic content in the aqueous and ethanolic *G. urbanum* rhizome extracts. As a result, ethanolic *G. urbanum* rhizome extract had a higher total phenolics content (2.22 ± 7.12 vs. 1.46 ± 7.85 mg gallic acid/mL extract) than aqueous *G. urbanum* rhizome extract. A review analyzing the constituents and pharmacology of *G. urbanum* found that, besides phenolic compounds, other categories of plant constituents, such as flavonoids and proanthocyanidins, have as well higher concentrations in the ethanolic extract as compared with the aqueous one (1261.5 vs. 768.2 GAE/L total phenols, 49.9 vs. 14.7 mg/L flavonoids, 60.1 vs. 37.5 mg/L proanthocyanidins) [43].

3.2 Optimized Synthesis Parameters

The AgNPs and AuNPs were synthesized by mixing, under continuous stirring, aqueous and ethanolic *G. urbanum* rhizome extracts with $AgNO_3$ and $HAuCl_4$ solutions. Several parameters involved in the MNPs biosynthesis reaction mechanism were tested by varying the metal precursor concentration, pH, ratio between plant extract and metal precursor volumes, temperature, and reaction time. All experiments were monitored by UV-Vis spectroscopy (Fig. 1), and the optimized synthesis conditions were selected based on the characteristics of the resulting UV-Vis spectra. The formation of MNPs is firstly indicated by a colour change of the synthesis mixture from light yellow to greyish-brown (AgNPs) and ruby-red (AuNPs). When excited by light, the collective oscillations of the free electrons at the surface of metallic Ag and Au generate absorption bands (Surface Plasmon Resonance – SPR band) in the visible domain at 400–500 nm (AgNPs) and 500–600 nm (AuNPs). The influence of the metal precursor over the synthesis process was studied by conducting experiments with $AgNO_3$ and $HAuCl_4$ solutions with concentrations varying between 1 and 5 mM. Overall, for both AgNPs (Fig. 1, A, B) and AuNPs (Fig. 1, C, D), the absorbance increased with the metal precursor concentration between 1 and 3 mM. At 5 mM $AgNO_3$, the SPR bands became broader and shifted to wide wavelengths, suggesting polydispersity and larger dimensions [65, 66] for the synthesized AgNPs. For AuNPs, using the 5 mM $HAuCl_4$ concentration impaired the synthesis. These results suggest that higher metal precursor concentrations do not confer benefits in aqueous and ethanolic *G. urbanum* rhizome extracts derived AgNPs and AuNPs synthesis. For both aqueous and ethanolic *G. urbanum* rhizome extracts derived AgNPs, the best characteristics for the SPR peak

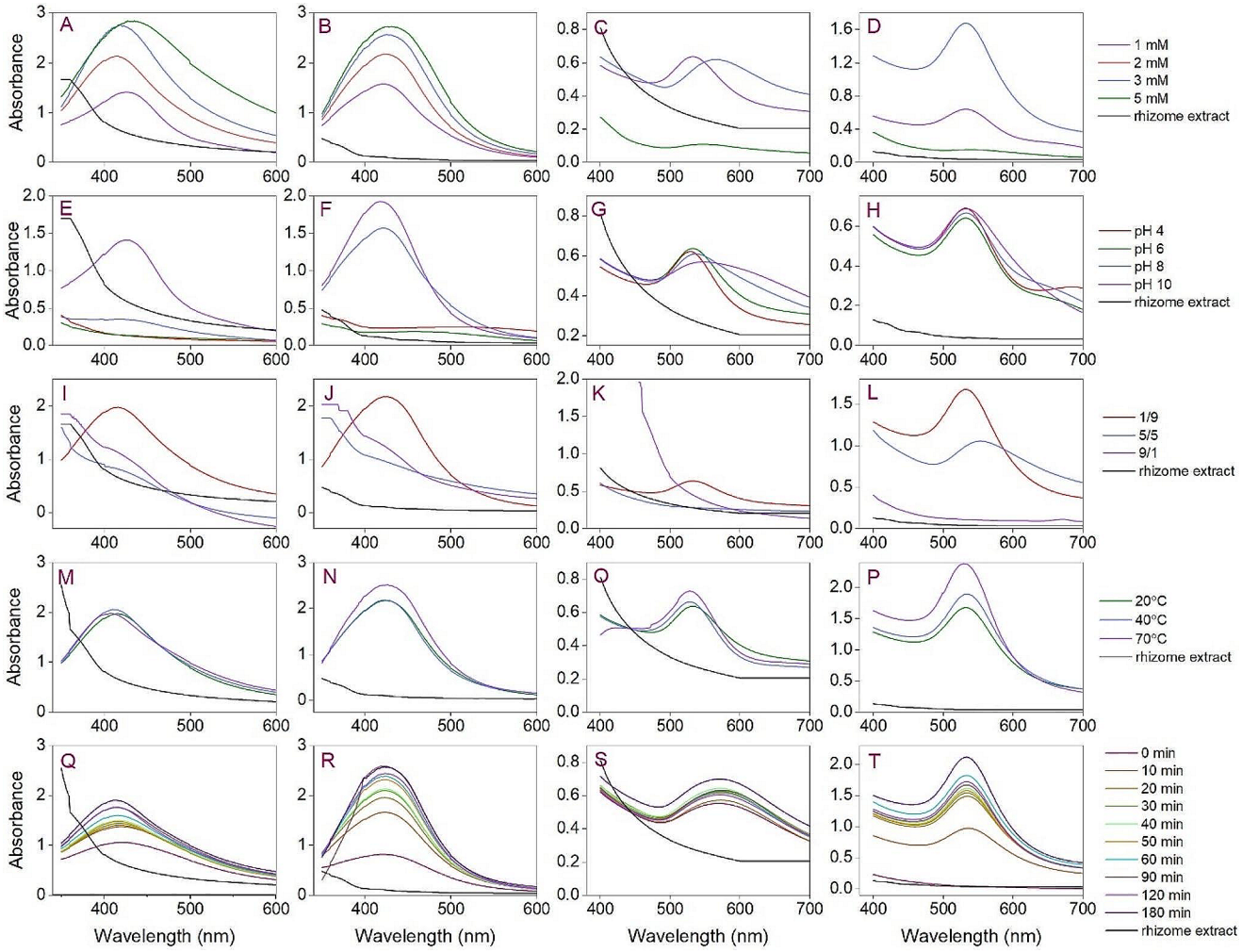


Fig. 1 Effect of $AgNO_3$ concentration, pH, ratio between the volumes of plant extract and $AgNO_3$, temperature, and reaction time on the synthesis of AgNPs from *Geum urbanum* aqueous (A, E,I, M,Q) and ethanolic (B, F,J, N,R) rhizome extracts; effect of $HAuCl_4$ concentration, pH, ratio between the volumes of plant extract and $HAuCl_4$, temperature, and reaction time on the synthesis of AuNPs from *Geum urbanum* aqueous (C, G,K, O,S) and ethanolic (D, H,L, P,T) rhizome extracts

(intensity, shape, wavelength) were obtained when the 3 mM $AgNO_3$ solution was used, which was selected as optimum for further analysis. The synthesis process differed for AuNPs when the aqueous rhizome extract was used, and the SPR peak had better characteristics for 1 mM $HAuCl_4$ concentration than for 3 mM $HAuCl_4$. Opposite, the ethanolic *G. urbanum* rhizome extract-derived AuNPs showed a higher and narrower SPR peak for 3 mM $HAuCl_4$ solution. Consequently, $HAuCl_4$ solutions of 1 mM (aqueous rhizome extract) and 3 mM (ethanolic rhizome extract) were considered optimum for AuNPs synthesis. Generally, the increase in metal salt concentrations generates higher MNPs yields, but above a certain limit, it may also lead to agglomeration, polydispersity, and yield decrease [67]. Moreover, higher metal salt concentrations (> 10 mM) are also associated with increased toxicity, which is a major drawback for biologically active MNPs production [66]. 1 mM metal salt concentration is often found optimal in studies of MNPs synthesized using plant extracts. However, there are cases when 3mM $AgNO_3$ was found optimal for the synthesis of spherical, small, and monodisperse AgNPs by using extracts from *Moringa oleifera* Lam. leaves (25.235 ± 0.694 nm) [52], *Potentilla fulgens* Wall. ex. Hook roots (15–20 nm) [53] and *Vernonia amygdalina* Delile leaves (63.08 nm) [68]. As for AuNPs, concentrations of $HAuCl_4$ varying between 1 and 3 mM were found optimal in synthesis with *Desmostachya bipinnata* (L.) Stapf [69], *Syzygium cumini* (L.) Skeels [70]). and *Gymnema sylvestre* R. Br. leaves [54] extracts.

Several other experiments were led to evaluate the influence of pH over the synthesis process by varying the extracts' pH values between 4 and 10. For AgNPs, the synthesis could not be achieved in an acidic medium (pH 4 and 6) for both *G. urbanum* rhizome extracts (Fig. 1, E, F), while AuNPs were attained in all the tested pH values (Fig. 1, G, H). With the aqueous *G. urbanum* rhizome extract, incipient AgNPs synthesis was observed at pH 6, while a sharper SPR peak appeared when pH 10 was employed. AgNPs synthesized using the ethanolic *G. urbanum* rhizome extract presented characteristic SPR peaks in a basic medium (pH 8 and 10). However, at pH 10, the SPR peak was sharper, and the absorption maxima slightly shifted to a shorter wavelength, suggesting the formation of smaller AgNPs. Therefore, pH 10 was selected as optimum for AgNPs synthesis with both types of *G. urbanum* rhizome extracts. Opposite, minor differences appeared on AuNPs spectra obtained in the various pH values tested; thus, the intrinsic extracts pH values were selected (pH 6). The alkaline conditions of the media promote the deprotonation of the hydroxyl moieties of the plant extract compounds, enhancing their reducing capacity, which results in higher yields in MNPs production. Moreover, an alkaline pH ensures a higher degree of stability for the synthesized MNPs that are also characterized by regular shapes, mainly spherical and hexagonal [55]. However, there are also cases when a neutral pH was found optimal for MNPs synthesis [66].

To evaluate the volume ratio between rhizome extract and metal precursor effects over the MNPs synthesis, several experiments (1:9, 5:5, and 9:1) were conducted, and the UV-Vis spectra were recorded (Fig. 1, I, J,K, L). For AgNPs and AuNPs synthesis with both rhizome extracts, the ratio 1:9 between plant extract and metal precursor showed the SPR peak with the best performances. Moreover, increasing the rhizome extract volume to the detriment of the metal precursor volume seems to impair the synthesis of both types of MNPs studied. Another study also found that the 1:9 ratio ratio between extracts from *Brassica nigra* (L.) W.D.J.Koch seeds, *Berberis vulgaris* L. roots and *Capsella bursa-pastoris* (L.) Medik, *Lavandula angustifolia* Mill, and *Origanum vulgare* Linnaeus leaves and the metal precursor is optimal for an increased accumulation of spherical MNPs [71].

The influence of temperature was evaluated by maintaining the reaction mixtures at 20, 40, and 70ºC. The synthesis of AgNPs using the aqueous *G. urbanum* rhizome extract proceeded similarly for all the tested temperatures (Fig. 1, M). The characteristic SPR peak appeared on the UV-Vis spectra, having an absorption maxima close to 400 nm. Therefore, the 20ºC temperature was selected in this case (absorption maxima at 416 nm). When the ethanolic *G. urbanum* rhizome extract was used for AgNPs synthesis, the SPR peaks were similar for the absorption maxima wavelength value (around 420 nm). However, the shape was observed to be different. As for 20 and 40ºC, the shape was similar; at 70ºC, the peak presented a broader shape, suggesting heterogeneous sizes. As a consequence, 20ºC was considered to be optimum for this case also. For synthesizing aqueous *G. urbanum* rhizome extract derived AuNPs, at 20ºC, the SPR peak appeared with an absorption maxima at 532 nm. As the temperature increased (40 and 70ºC), the absorption maxima slightly shifted to a shorter wavelength (538 nm), resulting in the conclusion of considering the 40 ºC as being optimum. When the different temperatures were employed in the ethanolic *G. urbanum* rhizome extract derived AuNPs synthesis, it was observed that as the temperature increases (20, 40, and 70ºC), the absorption maxima shifts to shorter wavelengths (534, 533, and 529 nm). Moreover, there is a large gap between the SPR peaks resulting at 40 and 70ºC, provided by a considerable difference in the intensities of the peaks (1.891 vs. 2.379 absorbances). Therefore, 70ºC was considered the optimum temperature for synthesizing ethanolic *G. urbanum* rhizome extract-derived AuNPs. Temperature represents an important factor that influences the synthesis process of MNPs. While an increased temperature enhances the molecule's

kinetic energy and facilitates the synthesis reaction, the process is beneficial up to a certain point, beyond which multiple collisions take place, generating aggregation and growth of MNPs [72]. Therefore, due to each plant extract specific composition, studies over the influence of temperature revealed various optimal conditions: 40 °C (*Tragopogon collinus* DC. whole plant extract derived AgNPs [73]), 45 °C (*Eucalyptus globulus* Labill. leaves extract derived AgNPs [74]), 55 °C (*Boswellia sacra* Flueck. leaves extract derived AgNPs [75]), 75 °C (*Hippophae rhamnoides* Linn. leaves extract derived AgNPs [76]) or 80 °C (*Hygrophila spinosa* T. Anders whole plant extract derived AuNPs [51]).

To evaluate the reaction time over the evolution of MNPs synthesis, the reaction mixtures of the samples in their optimum synthesis conditions determined in the previous experiments were maintained under continuous magnetic stirring for 180 min. The synthesis of AgNPs and AuNPs with both *G. urbanum* rhizome extracts started immediately after the mixture of the reactants (0 min) (Fig. 1, Q, R,S, T). At each time interval, the SPR peak was registered, having an absorption maxima at around 410 and 420 nm for AgNPs (aqueous and ethanolic *G. urbanum* rhizome extract, respectively) and 570 and 530 nm for AuNPs (aqueous and ethanolic *G. urbanum* rhizome extract, respectively). As a general consideration, for all samples, it can be seen that as the time interval allocated for magnetic stirring increases, so does the yield of the MNPs produced. However, the shapes and absorption maxima values may differ between samples, and by analyzing comparatively the UV-Vis spectra, the following time intervals were considered optimum: 180 min for aqueous *G. urbanum* rhizome extract derived AgNPs (1.902 absorbances at 413 nm), 40 min for ethanolic *G. urbanum* rhizome extract derived AgNPs (2.128 absorbance at 422 nm) and 180 min for aqueous and ethanolic *G. urbanum* rhizome extract derived AuNPs (0.697 absorbance at 570 nm and 2.115 absorbance at 533 nm, respectively). As a general consideration, prolonged time intervals allocated for the synthesis may result in the increase of both yield and polydispersity of MNPs [77]. Literature shows optimal time intervals that vary between 20 min and 72 h [78].

3.3 Characterization

3.3.1 FTIR Technique

Figure 2 illustrates the ATR-FTIR spectra of aqueous and ethanolic *G. urbanum* rhizome extracts and their derived AgNPs and AuNPs. FTIR spectroscopy was performed to identify the rhizome extracts' functional groups and the biomolecules involved in nanoparticle synthesis. All spectra showed broad peaks between 3239 and 3346 cm^{-1}, which are associated with N—H stretching vibration of the secondary amide functional groups in proteins [79–82]. Other studies suggest that the band at 3273 cm^{-1} belongs to the stretching vibration of O—H in alcohols/phenols [83–85]. Similarly, all sample spectra showed bands with

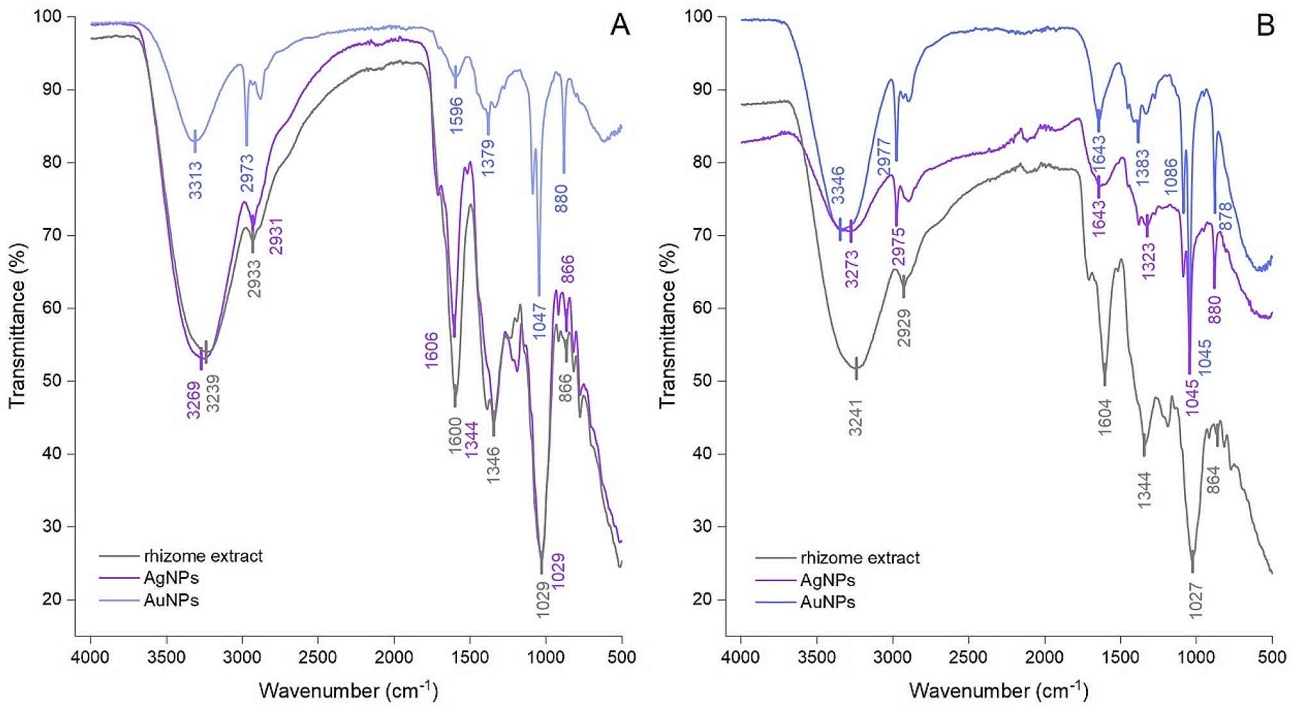


Fig. 2 ATR-FTIR spectra of aqueous (**A**) and ethanolic (**B**) *Geum urbanum* rhizome extracts and their derived AgNPs and AuNPs

peaks ranging between 2929 and 2977 cm^{-1} correlated with C—H stretching vibration of the methylene group [86–90]. The bands around 1600 cm^{-1} could be associated with N—H stretching vibrations in amines [91, 92] or the carbonyl (C = O) asymmetric stretching vibration in the amide I groups of proteins [93, 94]. Both rhizome extracts showed peaks around 1340 cm^{-1}, also present on their derived MNPs spectra shifted between 1323 and 1344 cm^{-1} (AgNPs) and 1379–1383 cm^{-1} (AuNPs). Various studies associated the 1344 cm^{-1} peak with alkene = C—H and nitrile N—O functional groups [95]. Sharp peaks between 1027 and 1086 cm^{-1} are characteristic of C—O—C stretching vibrations in carbohydrates. The band at 1027 cm^{-1} also correlates to the C—N or C—H stretching vibration of aliphatic amines or alkene, respectively [96, 97]. Peaks around 860–880 cm^{-1} indicated the presence of flavonoids in both rhizome extracts and derived MNPs, characteristic of the aromatic C—H out-of-plane bending vibrations [98]. AgNPs and AuNPs FTIR spectra show shifts and attenuation of the rhizome extracts' bands, suggesting the involvement of phytochemicals such as alcohols, phenols, proteins, and carbohydrates in the synthesis process, acting as reducing and stabilizing agents during the formation of MNPs. A similar study found two absorption peaks comparable to our results in bimetallic Ag/Au nanoparticles synthesized using *G. urbanum*, respectively, at 3324 and 1635 cm^{-1} [47]. The flavonoids and alkaloids from plant extract were frequently associated with synthesis and polyalcohols and terpenoids with stabilization [99].

3.3.2 DLS Technique

DLS analysis was used to assess the mean hydrodynamic diameter (z-average), PDI, and zeta potential of MNPs synthesized with aqueous (Fig. 3A) and ethanolic (Fig. 3B) *G. urbanum* rhizome extracts. These parameters are associated with solubility, physical stability, and biological activity performance [100]. Since the z-average considers a single value for each particle, the cumulant algorithm includes extreme values that do not always reflect the precise degree of heterogeneity. Therefore, the more appropriate statistic is PDI, depending on which population of particles may be classified as highly monodisperse (≤ 0.1) and moderately to highly polydisperse (0.1–0.4 and > 0.4, respectively) [101]. Thus, in the present case, the AgNPs dispersions show similar PDI values of 0.481 (aqueous extract) and 0.461 (ethanolic extract), indicating a high polydispersity degree. Similar PDI values have been previously reported [102–104]. Interestingly, the AuNPs dispersions showed different degrees of polydispersity between the aqueous and ethanolic rhizome extracts. A smaller value for PDI was obtained using the ethanolic rhizome extract in AuNPs synthesis (0.325) compared with the aqueous extract (0.557). The hydrodynamic diameter was significantly smaller for AgNPs and AuNPs synthesized with the ethanolic extract (41.14–46.26 nm, respectively) than those obtained with the aqueous extract (342.6–70.29 nm, respectively). The zeta potential values obtained for AgNPs were − 21.0 mV (aqueous rhizome extract) and − 18.8 mV (ethanolic rhizome extract). In comparison, AuNPs were characterized by -13,9 mV (aqueous

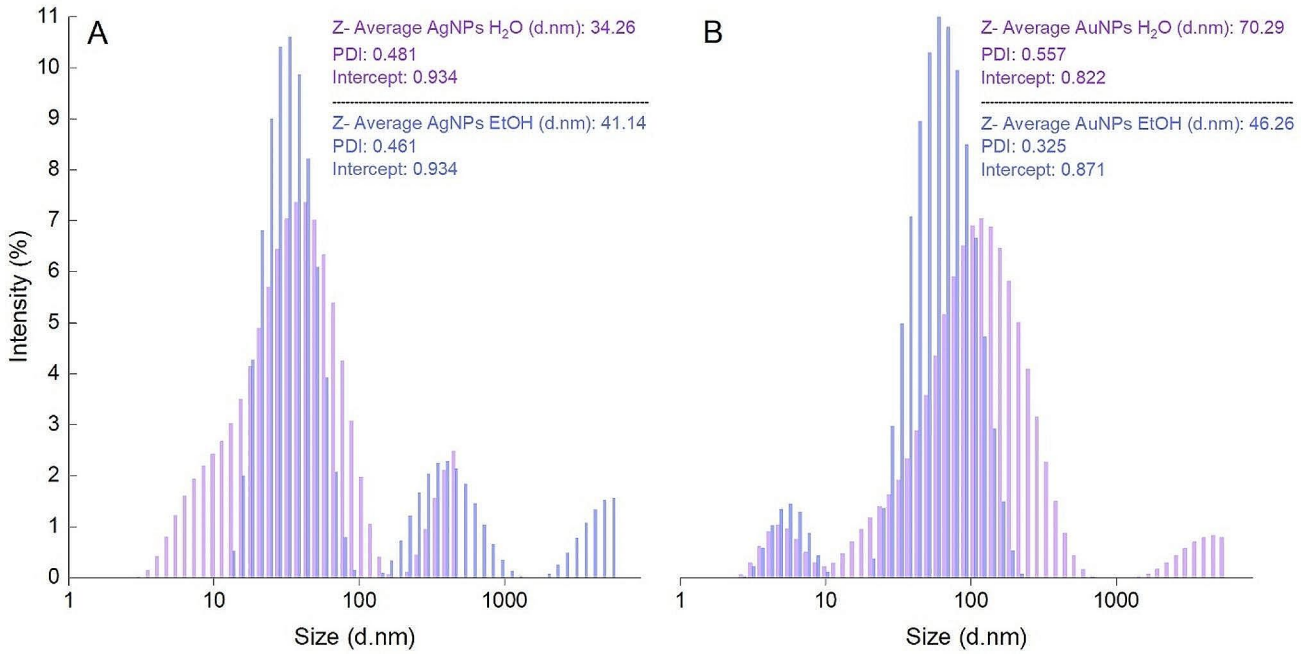


Fig. 3 DLS analysis of aqueous (violet bars) and ethanolic (blue bars) *Geum urbanum* rhizome extracts derived AgNPs (**A**) and AuNPs (**B**)

rhizome extract) and − 14,4 mV (ethanolic rhizome extract) values for zeta potential. As the zeta potential indicates the charge on the particle surface, it may indicate the stability in the dispersion of the colloid system. Agglomeration is prevented due to negative-negative repulsion, as zeta potential values of ± 10–20 mV suggest a relatively stable colloid system [88]. The results sustain the occurrence of rather neutral and relatively stable aggregates with time [105, 106]. Similar hydrodynamic diameter (39.5 nm) and zeta potential values (39.5 nm, and − 14.8 mV, respectively) were also obtained for *Brassica rapa* L. leaves extract derived AgNPs [107], properties that have a significant role in [107], preventing agglomeration and increasing the stability of the nanosystem [108].

3.3.3 SEM, EDX Technique

The morphological characteristics of AgNPs and AuNPs synthetized with aqueous and ethanolic *G. urbanum* rhizome extracts were evaluated using SEM analysis (Figs. 4B and D and 5B and D). High-resolution images captured at different magnifications were evaluated (10, 5, 2, and 1 µm). The results derived from the analysis emphasized that the synthesized AgNPs and AuNPs had aggregations of quasi-spherical nanoparticles of homogenous size distribution in the nano-size scale. The aqueous and ethanolic rhizome extracts used in MNPs synthesis performed differently, and images disclosed typical structures with a higher variability noticed between AgNPs and AuNPs aggregates. Figure 4A, C, and 5A, C illustrate the EDX analysis, showing the chemical composition and elemental distribution of AgNPs and AuNPs. In the case of AgNPs, a strong absorption peak was found around 3 keV, which is typical for silver monocrystals and confirms the reduction of silver ions to metallic silver [109]. Three distinct area evaluations were performed, and the mean value for mass and atom of each element occurred are presented in Table 1. Na and Mg are associated with the elemental profile of rhizome extract compounds [110]. The element Pt was also found in the evaluated spectra, which is associated with the contamination of samples that may have occurred during the preparation process. Peaks associated with chlorine, carbon, and oxygen were also present on the EDX spectra, belonging to the naturally occurring organic phytoconstituents of the rhizome extracts acting as capping

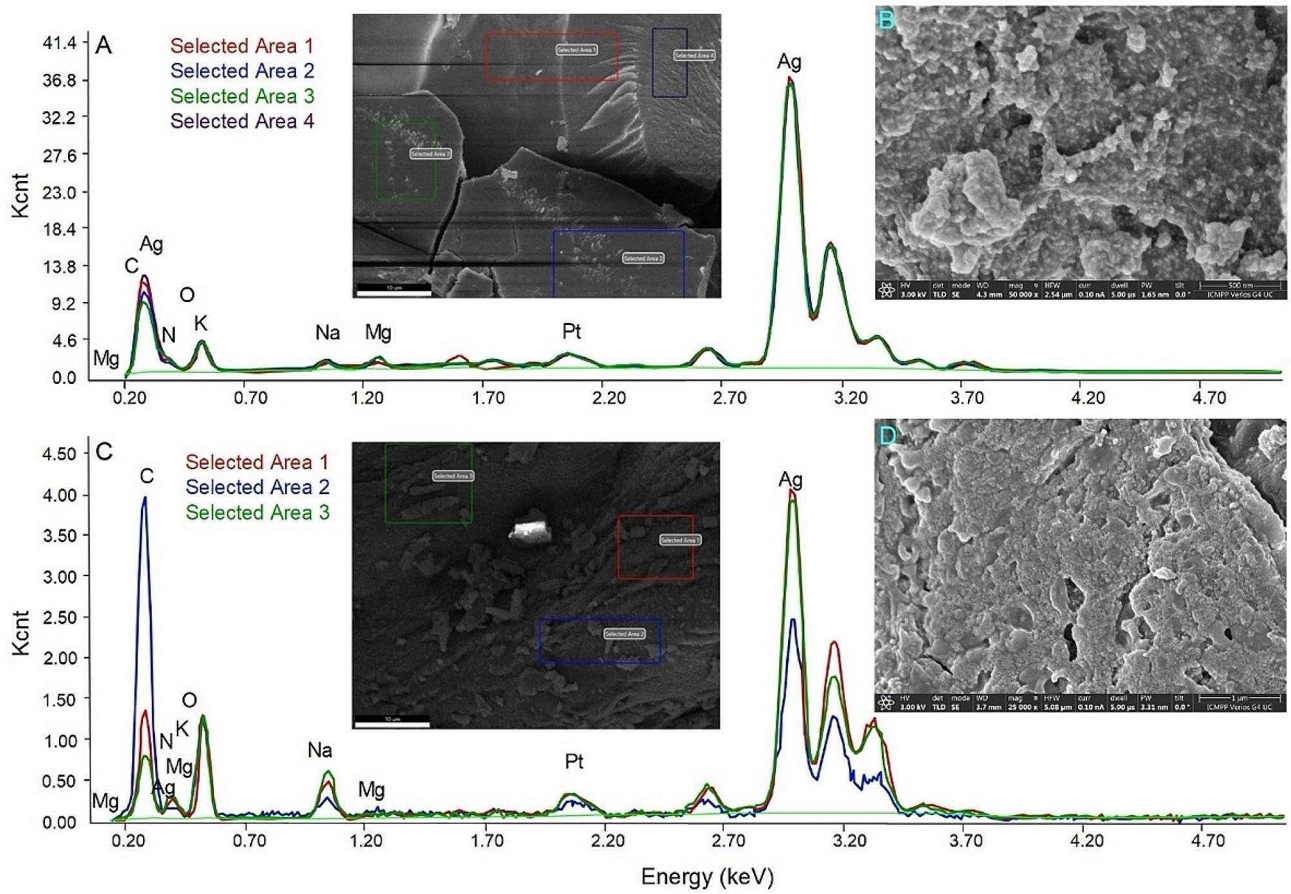


Fig. 4 Elemental composition (EDX) and SEM micrographs of aqueous *Geum urbanum* rhizome extract (**A**,**B**) and ethanolic *Geum urbanum* rhizome extract (**C**,**D**) derived AgNPs

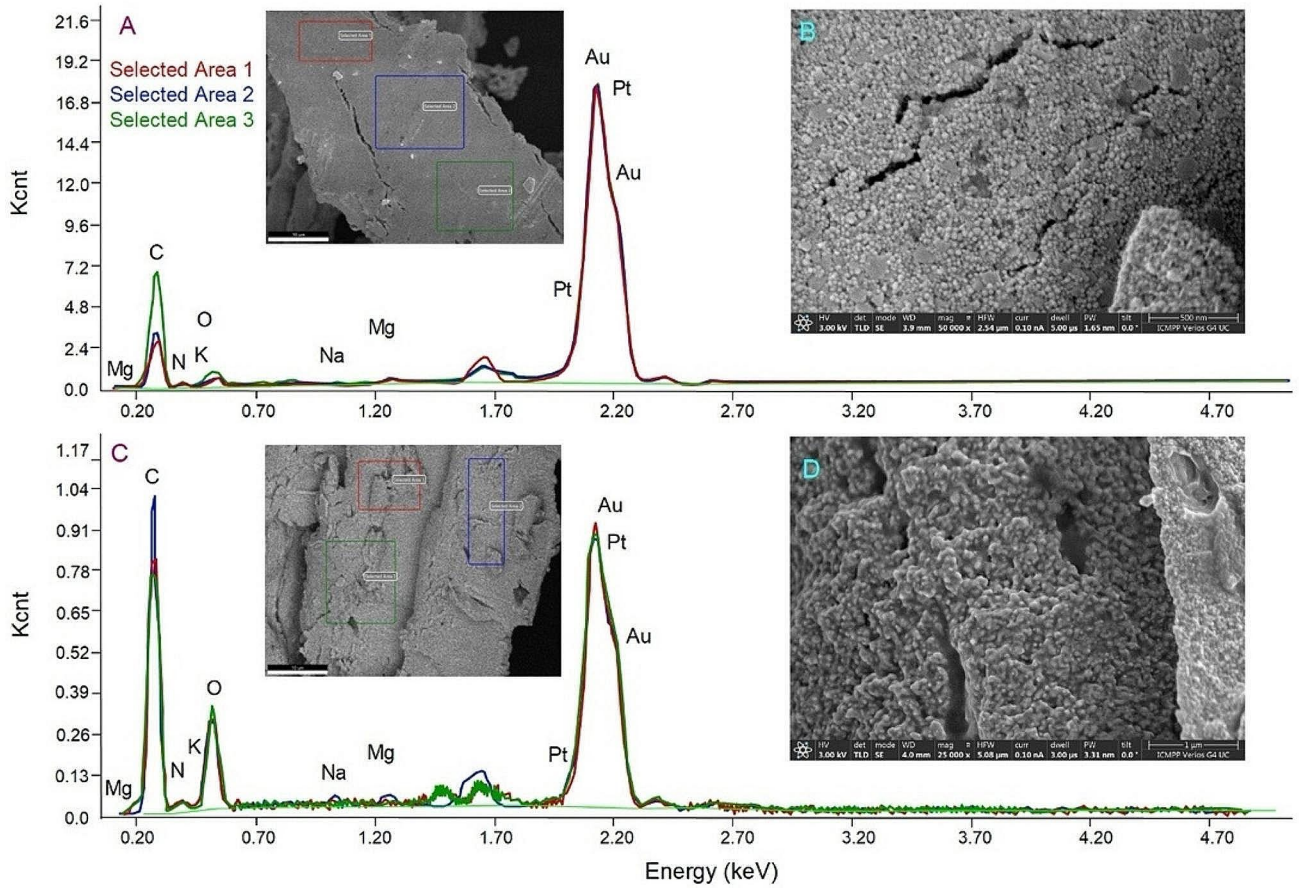


Fig. 5 Elemental composition (EDX) and SEM micrographs of aqueous *Geum urbanum* rhizome extract (**A**,**B**) and ethanolic *Geum urbanum* rhizome extract (**C**,**D**) derived AuNPs

Table 1 Elemental composition (EDX) of aqueous and ethanolic *Geum urbanum* rhizome extracts derived AgNPs and AuNPs

	aqueous rhizome extract derived AgNPs		ethanolic rhizome extract derived AgNPs		aqueous rhizome extract derived AuNPs		ethanolic rhizome extract derived AuNPs	
Element	Mass %	Atom %	Mass %	Atom %	Mass %	Atom %	Mass %	Atom %
C	12.70	37.75	18.97	39.83	9.57	56.20	31.67	68.57
N	2.63	6.70	3.90	7.83	0.87	4.43	2.23	4.13
O	12.43	27.65	20.03	34.83	1.37	6.03	11.90	19.40
Na	2.00	3.20	3.97	5.03	0.13	0.40	0.47	0.50
Mg	1.25	1.90	0.33	0.33	0.20	0.57	0.30	0.33
Ag	65.25	21.88	37.27	9.97	-	-	-	-
Au	-	-	-	-	83.30	30.63	48.03	6.33
Pt	3.55	0.68	15.50	2.13	4.63	1.70	5.40	0.70

agents for AgNPs [111, 112]. The gold chloroaurate bioreduction to elemental Au was confirmed by a strong absorption signal at a 2.2 keW energy level [14]. Several other signals were noted, including platinum, carbon, oxygen, potassium, magnesium, and sodium, which are also found in AgNPs, indicating similar origins, mainly corresponding to the phytochemicals in rhizome extracts. In the elemental composition as masses percentages, Ag and Au represent the major elements in AgNPs (65.25% in aqueous rhizome extract-derived AgNPs and 37.27% in ethanolic rhizome extract-derived AgNPs), and AuNPs, respectively (83.30% in aqueous rhizome extract derived AuNPs and 48.03% in ethanolic rhizome extract derived AuNPs) (Table 1). Both AgNPs and AuNPs showed a different elemental distribution between the aqueous and ethanolic rhizome extracts, being observed that a higher mass percentage for Ag and Au were obtained in the case of the aqueous extract (65.25 vs. 37.27% for AgNPs and 83.30 vs. 48.03% for AuNPs).

3.3.4 TEM Technique

AgNPs and AuNPs size distribution and morphological characteristics were achieved through TEM imaging. The biogenic AgNPs prepared with *G. urbanum* rhizome extracts were pseudo-spherical particles, having similar diameters ranging between 4.09 and 24.66 nm with a mean of 9.82 ± 3.68 nm (aqueous rhizome extract, Fig. 6, A) and 4.89 and 24.44 nm with a mean of 14.29 ± 3.46 nm (ethanolic rhizome extract, Fig. 6, B). Aqueous and ethanolic *G. urbanum* rhizome extract-derived AgNPs sizes showed comparable variance, 13.59 and 12.01 nm, respectively, indicating dimensions close to the mean for all nanoparticles. AuNPs showed a variety of shapes, including quasi-spherical, polygonal, and triangular. The dimensions varied considerably between aqueous (8.18–60.85 nm) and ethanolic (5.08–42.97 nm) *G. urbanum* rhizome extract-derived AuNPs. A clear difference was observed for the mean nanoparticle sizes of the aqueous and ethanolic *G. urbanum* rhizome extract-derived AuNPs (24.89 ± 10.75 and 15.88 ± 6.28 nm, respectively), while the variance also differed significantly from 115.71 to 39.51 nm, respectively, indicating high polydispersity. In both cases, it was noted that around 25% of MNPs had particle sizes above the third quartile, therefore being assimilated as outliers. Even so, under close evaluation of TEM images, we can observe that direct contact between nanoparticles and the bigger formations, considered outliers, is observed only in several cases. Also, the absence of an organic layer at the nanoparticle surface could suggest that the smaller nanoparticles coagulate, resulting in more extended formations. In our experiments, to sustain that larger nanoparticles are not aggregates, we can mention that the shape is similar to smaller ones. Thus, we used D'Agostino K-Squared and Shapiro-Wilk normality tests to evaluate nanoparticle size distribution from the four datasets. The results show that the aqueous *G. urbanum* rhizome extract-derived AgNPs data are not significantly drawn from a normal distribution and rejected the normality ($p < 0.0001$), compared to the ethanolic *G. urbanum* rhizome extract-derived AgNPs, which demonstrated a normal distribution ($p = 0.11$). Analyzing the AuNPs nanoparticle size distribution, we noted a rejection of normality in both samples ($p < 0.0001$). Thus, a log-normal distribution to smooth the datasets was applied based on a positively skewed long right tail. The log-normal distribution emphasized a certain degree of inflexibility on several points, showing the significant variability of nanoparticle sizes, usually explained by natural phenomena. The scientific reports discussed that the shape and size of nanoparticles are essential in biological activity since smaller nanoparticles are easily transferred

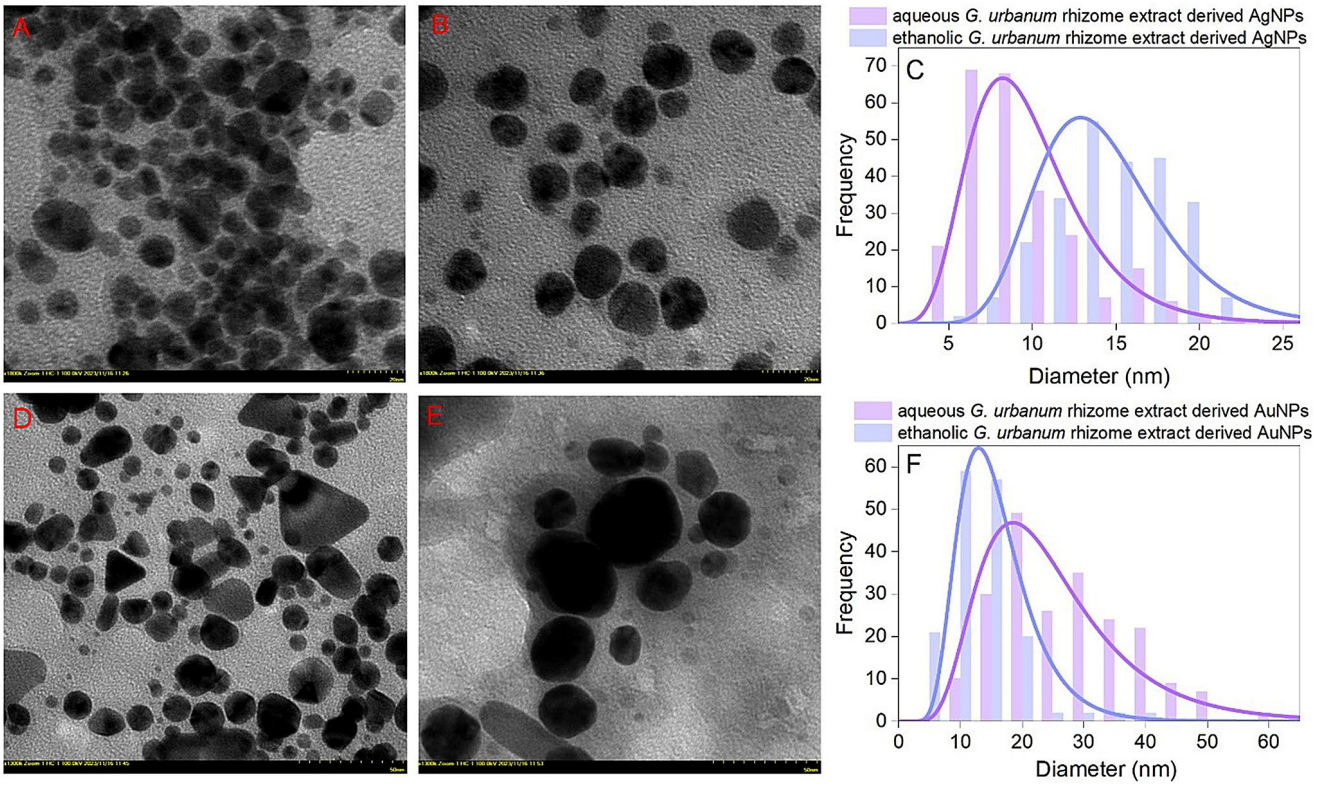


Fig. 6 Aqueous *Geum urbanum* rhizome extract derived: AgNPs – TEM images (**A**) and size distribution histogram (**C**) and AuNPs – TEM images (**D**) and size distribution histogram (**F**); ethanolic *Geum urbanum* rhizome extract derived: AgNPs – TEM images (**B**) and size distribution histogram (**C**) and AuNPs – TEM images (**E**) and size distribution histogram (**F**)

through bacteria cell membranes [113]. Even so, choosing only one nanoparticle size category is challenging, considering the aggregation phenomena of small particles in complex aggregates [114]. In the present case, the aqueous and ethanolic *G. urbanum* rhizome extract-derived AgNPs and AuNPs shape and sizes had a certain degree of variability, which was further tested for biological activity to assess their performance.

3.4 Biological Activity

3.4.1 Antimicrobial Assay

The antimicrobial potential of AgNPs and AuNPs was investigated by disc diffusion assay against Gram-positive (methicillin-susceptible *Staphylococcus aureus* (MSSA), methicillin-resistant *Staphylococcus aureus* (MRSA), *Staphylococcus epidermidis*) and Gram-negative (*Escherichia coli, Pseudomonas aeruginosa, Klebsiella pneumoniae*) bacteria and yeasts (*Candida albicans*). The results are presented in Table 2.

Both AgNPs and AuNPs demonstrated a more intense toxicity against Gram-positive bacteria, the most significant growth inhibition zones being observed against *S. aureus* MSSA. It is worth noting that the activity of all the MNPs against *S aureus* MRSA was comparable and even higher than the one developed by gentamicin (7.57 ± 0.58 mm). The aqueous *G. urbanum* rhizome extract-derived AgNPs and AuNPs were more active against *S. epidermidis* (12.00 ± 1 and 13.33 ± 1.15 mm, respectively), as compared with ethanolic *G. urbanum* rhizome extract derived AgNPs and AuNPs (9.00 ± 1.73, and 6.00 ± 1.00 mm, respectively). Regarding the Gram-negative bacteria, better results were obtained against *P. aeruginosa* for all the MNPs studied. All samples developed a modest antifungal activity against *C. albicans.* AgNPs are well-known antimicrobial agents active against various pathogens, and the mechanisms involved are still less understood. However, it is proposed that AgNPs may adhere to the microbial cell surface through electrostatic interactions, causing damage to the cell membrane and penetrating the cell by binding with essential protein structures. Here, they develop severe cell metabolism malfunctions that lead to cell death. It is also stated that by phyto-functionalization nanoscale silver, which is mainly toxic for Gram-negative bacteria, the antibacterial activity of these plant extract-derived AgNPs is extended against Gram-positive germs as well [115, 116]. For the antimicrobial activity of AuNPs, a similar mechanism of binding to the bacterial cell membrane seems to be involved, but without causing cellular death [117]. However, both AgNPs and AuNPs possess higher affinity for phosphorus and sulfur moieties in proteins and tend to form bonds with nitrogen and oxygen. Moreover, another mechanism responsible for the antimicrobial activity of AgNPs and AuNPs is considered to be ROS production, which is further responsible for causing severe disruptions to the microbial cell, such as loss of the membrane cell integrity, alterations of the respiratory activity, and DNA damage [118]. In our study, more intense antimicrobial activity occurred for AgNPs than AuNPs, which may be attributed to the intrinsic antimicrobial activity of Ag as well as a correlation with the shape of MNPs. Due to an enhanced rate of cellular uptake, the spherical-shaped MNPs (AgNPs) seem to present a better antimicrobial activity than other shapes (AuNPs) [119, 120]. However, the antimicrobial activity for the herein synthesized AuNPs was also considerable, which may be attributed to the sharp edges of their shapes (triangular, polygonal) distorting the bacterial cell membrane [119]. Differences noted between the intensities of antimicrobial activities of the aqueous and ethanolic *G. urbanum* rhizome extract-derived AgNPs and AuNPs suggest the significant role of extracts' phytochemicals situated at the MNPs surface as capping agents in developing the MNPs toxicity against pathogens. For example, catechin and tormentic acid were isolated from an ethanolic *G. urbanum* rhizome extract, providing remarkable toxicity against Gram-positive bacteria *S. aureus* ATCC 3359, defined by MIC values of 0.25 and 0.125 mg/mL, respectively. Catechin was also

Table 2 Diameters of inhibition zones (mm) against pathogenic bacteria and yeasts obtained for aqueous and ethanolic *Geum urbanum* rhizome extracts derived AgNPs and AuNPs. The statistical difference between ethanolic and aqueaous AgNPs and AuNPs was tested, and no significant differences were found for $p < 0.05$

Microorganism	Nystatin	Gentamicin	aqueous extract - AgNPs	ethanolic extract - AgNPs	aqueous extract - AuNPs	ethanolic extract - AuNPs
S. aureus ATCC 25,293 (MSSA)	ND	23.00 ± 0.58	9.67 ± 0.58	14.67 ± 0.58	11.00 ± 0.58	7.00 ± 0.58
S. aureus ATCC 43,300 (MRSA)	ND	7.57 ± 0.58	6.25 ± 1.15	8.27 ± 1.73	6.50 ± 0.58	6.85 ± 0.58
S. epidermidis ATCC 12,228	ND	29.87 ± 1.15	12.00 ± 1	9.00 ± 1.73	13.33 ± 1.15	6.00 ± 1
E. coli ATCC 25,922	ND	19.23 ± 0.58	6.33 ± 0.58	6.33 ± 0.58	9.33 ± 0.58	6.50 ± 1.15
K. pneumoniae ATCC 13,883	ND	20.33 ± 0.58	6.33 ± 0.58	6.25 ± 1.15	6.33 ± 1.15	6.20 ± 0.58
P. aeruginosa ATCC 9027	ND	22.89 ± 0.58	9.67 ± 0.58	7.67 ± 0.58	7.87 ± 0.58	8.25 ± 0.58
C. albicans ATCC 90,028	21.33 ± 0.58	ND	6.25 ± 1.73	7.25 ± 0.58	7.25 ± 0.58	6.00 ± 1

ND: not determined

responsible for bactericidal activity against *P. aeruginosa* 6749 (MIC = 0.5 mg/mL) [44].

3.4.2 Antioxidant Activity

Figure 7A, B,C, D shows the dose-dependent inhibitory activities of the biosynthesized AgNPs and AuNPs with aqueous and ethanolic *G. urbanum* rhizome extracts, using lipoxygenase inhibition (LOX), DPPH radical scavenging, metal ion chelating activity, and hydroxyl radical generation assays. For all the tests, the inhibitory activities were concentration-dependent for both aqueous and ethanolic *G. urbanum* rhizome extracts and their derived MNPs.

3.4.3 In Vitro Lipoxygenase Inhibition (LOX) Assay

The inhibition of lipoxygenase activity of the extracts and derived AgNPs and AuNPs was observed as a decrease of absorbance at 234 nm due to a less formation of hydroperoxylinoleic acid through blocking the linoleic acid oxidation process [121]. Our results showed significant LOX inhibition (> 50%) for concentrations higher than 1.25 mg/mL only for the ethanolic *G. urbanum* rhizome extract-derived AuNPs and AuNPs. Over 2.5 mg/mL, all samples proved significant LOX inhibition activities, except for the aqueous *G. urbanum* rhizome extract (Fig. 7A). The compounds identified in the aqueous extract reduce the enzyme's activity but do not ensure a level of inhibition over 50% due to their lower extraction rate in the aqueous medium compared with the ethanolic one. The extract inhibition capacity is directly correlated with their content in polyphenols; thus, the ethanolic rhizome extract contains a 1.5 times greater amount of phenols as compared with the aqueous one (2.22 ± 7.12 vs. 1.46 ± 7.85 mg gallic acid/mL extract). The EC_{50} value was evaluated to assess the sample concentration required to inhibit 50% of a radical, a lower value associated with higher antioxidant activity of the sample [122]. According to the EC_{50} values and the scale proposed by Phongpaichit et al. [123] the ethanolic *G. urbanum* rhizome extract-derived AgNPs exhibited the most intense antioxidant activity (34.20 µg/mL). An intermediate antioxidant activity was found for ethanolic *G. urbanum* rhizome extract-derived AuNPs (58.51 µg/mL), ethanolic *G. urbanum* rhizome extract (74.05 µg/mL), and aqueous *G. urbanum* rhizome

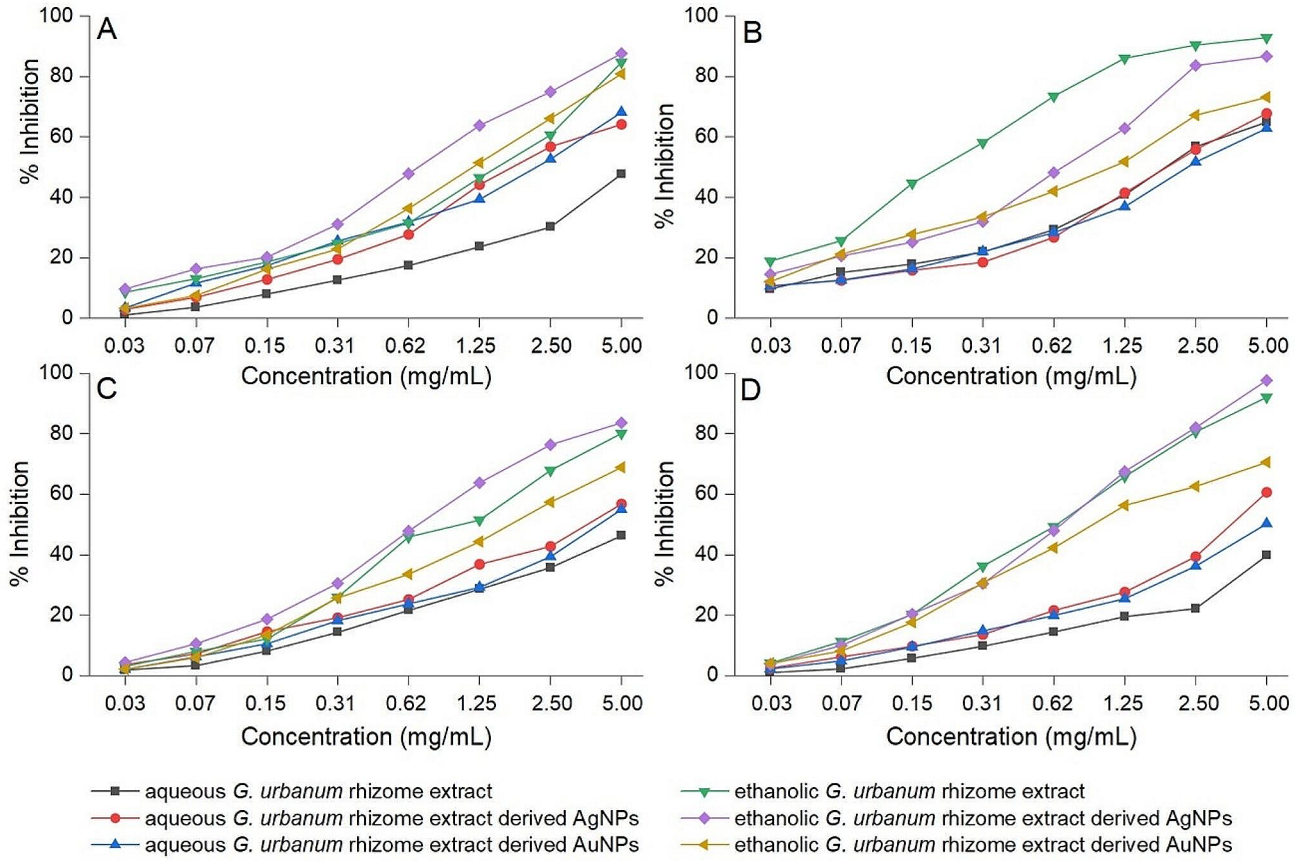


Fig. 7 **A** – lipoxygenase inhibition assay; **B** – DPPH radical scavenging test; **C** – metal ion chelating activity ; **D** – hydroxyl radical generation. The statistical difference between aqueous and ethanolic *G. urbanum* extracts and their derived AgNPs and AuNPs were tested, and no significant differences were found for $p < 0.05$

extract-derived AgNPs (86.35 µg/mL). Weak antioxidant activity was associated with aqueous *G. urbanum* rhizome extract-derived AuNPs (109 µg/mL). Between the two types of extracts used in MNPs synthesis, it was observed that the ethanolic *G. urbanum* rhizome extract–derived AgNPs/AuNPs showed superior inhibitory activity. Moreover, all the synthesized MNPs were more active than the extracts used for their preparation. The inhibitory activities of the samples may be determined by blocking the enzyme iron ion to participate in the redox process (through chelation or reduction), altering the active center structure, or changing the spatial structure of the enzyme. The –OH groups of the phenolic compounds in the rhizome extracts, also attached on the MNPs surface as capping agents, may interact with the redox reaction catalyzed by the enzyme and neutralize the intermediately formed lipid peroxides. Moreover, the hydroxyl groups may be responsible for chelating the ferrous ion from the enzyme's active center or reducing the ferric ion after the enzyme has oxidized the substrate [124]. Other studies highlighted the involvement of polyphenols in the lipoxygenase inhibition process [125, 126]. AgNPs nanoparticles using extracts of *Penicillium* sp. isolated from *Glycosmis mauritiana* (Lam.) Tanaka showed a potent inhibition of lipoxygenase enzyme (68%) [127]. In a similar study, AgNPs synthesized using an aqueous *Calophyllum tomentosum* Wight leaf extract showed an antilipoxygenase inhibitory activity of 71.52% [128]. Aqueous *Sambucus wightiana* L. whole plant extract-derived AuNPs showed a significant activity of LOX enzyme inhibition (EC_{50} = 30.64 µg/mL), which was more efficient than the aqueous *S. wightiana* whole plant extract activity (EC_{50} = 37.35 µg/mL) [129].

3.4.4 DPPH Radical Acavenging Activity

The DPPH radical scavenging assay evaluates the capability of the tested compounds to stabilize the synthetic and unstable 2,2-diphenyl-1-picryl-hydrazyl (DPPH) radical. DPPH is an active free radical (purple colour) that reacts with electrons or hydrogen donors, resulting in a diamagnetic molecule, thus being capable of evaluating the sample's antioxidant activity [130]. The reducing compounds neutralize the DPPH radical, concomitant with a colour change from violet to yellow and a decrease in absorbance values registered at 517 nm. A reduced DPPH is associated with a less purple color in the sample and a higher free-radical scavenging capacity of an antioxidant compound [131]. In the present study, inhibition of DPPH radical varied poorly from concentrations of 2.5 to 5 mg/mL for *G. urbanum* rhizome aqueous samples, e.g., 56.72 to 64.95% (extract), 55.85 to 67.89% (extract-derived AgNPs), and 51.74 to 62.88% (extract-derived AuNPs). The DPPH free radical scavenging activity of ethanolic *G. urbanum* rhizome extract increased from 58.17 (0.31 mg/mL) to 92.85 (5 mg/mL) percent of inhibition, compared with aqueous rhizome extract, which varied from 56.72 (2.5 mg/mL) to 64.95% (5 mg/mL) (Fig. 7B). The lowest EC_{50} value was found in ethanolic *G. urbanum* rhizome extract (20.51 µg/mL), indicating an intense antioxidant activity. Moderate antioxidant activity was observed for ethanolic *G. urbanum* rhizome extract-derived AgNPs (67.99 µg/mL). For other samples, the EC_{50} value exceeded 100 µg/mL, performing weak antioxidant activity. The intense antioxidant activity can result from different functional groups discussed in FTIR analysis responsible for the bio-reduction of Ag^{+} and Au^{3+} to MNPs. MNPs showed a lower capacity to neutralize the DPPH radical than the extracts used in their synthesis. The differences are more significant for the ethanolic rhizome extract, with the scavenger activity decreasing by 3 (AgNPs) and 5 (AuNPs) times. The neutralization of the DPPH radical is achieved by the hydrogen and electron donor groups (hydroxyl groups) from the composition of rhizome extracts or attached to the surface of MNPs. The participation of these functional groups in the reduction of metals and MNPs synthesis may explain the lower intensity of the scavenger effect of nanoparticles compared to the extracts. The scavenger activity depends on the extract concentration, and similar to the results presented in other studies, the ethanolic extract showed the most intense effect [132, 133]. A recent study regarding AgNPs and AuNPs phyto-functionalized with an aqueous *Opuntia ficus-indica* (L.) Mill. whole plant extract indicated similar DPPH scavenging activities, higher in AgNPs (52.25–57.50%) compared with AuNPs (37.07–59.07%) [134]. The AgNPs synthesized using an ethanolic *Filago desertorum* Pomel whole plant extract showed a DPPH scavenger activity of 72.51% (EC_{50} = 144.61 µg/mL) [135]. In contrast, AgNPs and AuNPs synthesized using *Mentha spicata* L. essential oil had an DPPH inhibition percent of 57.20 and 38.90%, respectively, at 100 µg/mL [136].

3.4.5 Metal Ion Chelating Activity Assay

Figure 7C shows the Fe^{2+} chelating activities of the rhizome extracts and derived MNPs. In the presence of ferrozine, Fe^{2+} forms a pink-colored complex with a maximum absorbance of 562 nm. The absorbance of this complex is diminished if the reaction media contains chelating agents [57]. The maximum Fe^{2+} chelating activity was observed for ethanolic *G. urbanum* rhizome extract-derived AgNPs, which increased from 63.84 (1.25 mg/mL) to 83.6% (5 mg/mL). At 5 mg/mL, the Fe^{2+} ion chelating ability decreased in the following order: ethanolic *G. urbanum* rhizome extract (80.16%), ethanolic *G. urbanum* rhizome extract-derived

AuNPs (68.94%), aqueous *G. urbanum* rhizome extract-derived AgNPs (56.76%), aqueous *G. urbanum* rhizome extract-derived AuNPs (54.95%), and aqueous *G. urbanum* rhizome extract (46.24%). The EC_{50} values indicate weak antioxidant activities, best of all being calculated for ethanolic *G. urbanum* rhizome extract-derived AgNPs (137 µg/mL). Fe^{2+} is essential for the hemoglobin structure, oxygen transport process, ATP synthesis, and other cellular biochemical pathways. It shows increased reactivity and is involved in the redox process, thus producing ROS. Fe^{2+} participates in the Fenton and Haber-Weiss reactions through which hydroxyl and superoxide anion radicals are generated. These radicals show very high chemical reactivity, initiating oxidation reactions, especially for the unsaturated compounds, thus altering the cell membranes or other biologically relevant compounds [137]. Thus, the chelation of Fe^{2+} impairs the synthesis of SRO. Plant extracts contain polyphenols that, through their functional groups, can chelate the ferrous ions, or they may firstly reduce Fe^{3+} to Fe^{2+}, followed by chelation [58, 138–140]. The phyto-functionalization of MNPs with vegetal polyphenols explains their ability to chelate Fe^{2+}, such MNPs being, therefore, useful to combat an excess of ferrous ions in a biological environment [141]. The ability of MNPs to chelate Fe^{2+} may be higher than the plant extract used in their synthesis [141]. This may explain the lower EC_{50} values calculated for AgNPs phyto-functionalized with both types of *G. urbanum* rhizome extracts compared to those used in their synthesis. AuNPs proved to be less effective. The chelating capacity of ethanolic extract-derived AgNPs was approximately 2.5 times higher than the one obtained for ethanolic extract-derived AuNPs, while for the aqueous extract, the difference was much smaller. The metal-phyto-compound interaction and the physicochemical characteristics of each type of MNPs may determine the different activity of AgNPs and AuNPs. Another study found Fe^{2+} ion chelating ability for biosynthesized AgNPs by *Artemisia haussknechtii* Boiss. and *Nothapodytes nimmoniana* (J.Grah.) D.j. Mabberley fruit extracts had an inhibition percent of 68.93 [142] and 98.41 mg/g extract, respectively [143]. Another survey investigated the metal chelating activity of ethanolic and aqueous *Terminalia arjuna* (Roxb.) Wight & Arn. bark extracts-derived AuNPs and AgNPs, resulting in a better performance for AuNPs synthesized with ethanolic extract [144]. The authors considered the high gold electron-transferring ability the principal reason for better performance [144]. However, in our study, the ethanolic extract also proved to have better chelating activity than the aqueous one. However, the ethanolic extract-derived AgNPs showed more significant activity (Fig. 7C).

3.4.6 Hydroxyl Radical Scavenging Assay

Figure 7D illustrates the hydroxyl radical scavenging activity of ethanolic and aqueous *G. urbanum* rhizome extracts and biosynthesized MNPs. At concentrations of 1.25 and 5 mg/mL, the ethanolic rhizome extract showed a more intense inhibition of the hydroxyl radical (65.85 and 92.08%, respectively) than the aqueous rhizome extract (19.46 and 39.74%, respectively). The highest percentage of inhibition registered at 5 mg/mL occurred for the ethanolic *G. urbanum* rhizome extract-derived AgNPs (97.71%), followed by the ethanolic *G. urbanum* rhizome extract (92.08%) and ethanolic *G. urbanum* rhizome extract-derived AuNPs (70.59%). Based on the ANOVA one-way test for mean comparison, the ethanolic extract and derived MNPs differ significantly ($p < 0.05$) from the aqueous rhizome extract and derived MNPs. The ethanolic *G. urbanum* rhizome extract had the highest hydroxyl radical scavenging activity with the lowest EC_{50} value (145.28 µg/mL), followed by ethanolic *G. urbanum* rhizome extract-derived AgNPs (151.13 µg/mL). Neutralization of the hydroxyl radicals is achieved by species capable of donating protons and electrons, such as the –OH groups from polyphenols. The presence of these polyphenols in greater quantity in the ethanolic extract, compared with the aqueous one, explains the greater efficiency of the ethanolic extract (neutralization capacity over 90%) compared to the aqueous one (neutralization capacity below 50%). In the hydro-alcoholic and aqueous extracts, the glycosylated forms of polyphenols prevail, compared to the alcoholic extracts in which aglycones predominate, containing several free –OH groups available for reducing process. Fe^{2+} is involved in the synthesis of the hydroxyl radical. Thus, the chelation of this ion blocks the hydroxyl radical pathway of synthesis [140]. This mechanism explains the ability of plant extracts and derived MNPs to neutralize the hydroxyl radical and reduce its synthesis. The difference in the effectiveness of the samples in the Fe^{2+} chelation test and hydroxyl radical scavenging assay is determined by the different chemical composition of the two extracts, particular physicochemical properties of MNPs, and types of extracts' phytochemicals attached at the MNPs surface. Moreover, the two tests are performed at different pH, influencing the functional groups' ionization. Several other studies reported hydroxyl radical scavenging activities for different plant extracts and derived AgNPs, e.g., *Helicteres isora* L. root extract [145], *Cleistanthus collinus* (Roxb.) Benth. Ex Hook. f. leaf extract [146], *Parrotiopsis jacquemontiana* (Decne.) Rehder leaf extract [147], or *Shorea roxburghii* G. Don stem bark extract [148]. AuNPs synthesized using an aqueous *Solanum nigrum* L. leaf extract showed higher hydroxyl radical (66%) inhibition rates than aqueous *S. nigrum* extract used in synthesis (43%) [149].

Also, the aqueous *Couroupita guianensis* Aubl. fruit extract had a maximum percentage of inhibition (89.2%), which was higher than the one obtained for the derived AuNPs (70.06%) [150].

4 Conclusions

The study reveals that aqueous and ethanolic *G. urbanum* rhizome extracts can be use to synthesize biogenic AgNPs and AuNPs. Total phenolic contents showed a higher value for the ethanolic extract compared to the aqueous. FTIR spectra analysis indicates that during MNP formation, phytochemicals such as alcohols, phenols, proteins, and carbohydrates from the rhizome extracts have reducing and stabilizing roles. Based on DLS measurements, the MNPs hydrodynamic diameters were smaller for AgNPs than AuNPs. The negative zeta potential values suggest that relatively stable colloid systems were obtained due to negative-to-negative repulsion that prevents the formation and agglomeration of nanostructures. According to TEM data, MNPs diameters varied insignificantly for aqueous and ethanolic rhizome extract-derived AgNPs (between 4.09 and 24.66, and 4.89 and 24.44 nm, respectively), compared with AuNPs (between 8.18 and 60.85, and 5.08 and 42.97 nm, respectively). Also, the polydispersity of aqueous and ethanolic nanoparticles was significant only in the case of aqueous and ethanolic rhizome extract-derived AuNPs (115.71 and 39.51 nm, respectively). According to the antimicrobial assay, AgNPs and AuNPs performed better against Gram-positive bacteria, showing the most significant growth inhibition zones against methicillin-susceptible *S. aureus* (DZI of 14.67 ± 0.58 mm obtained for ethanolic *G. urbanum* rhizome extract derived AgNPs). MNPs demonstrated significant LOX inhibition activities, with the most intense antioxidant activity for ethanolic *G. urbanum* extract-derived AgNPs ($EC_{50} = 34.20$ µg/mL) and AuNPs ($EC_{50} = 58.51$ µg/mL). DPPH assay illustrated the lowest EC_{50} value for ethanolic *G. urbanum* rhizome extract (20.51 µg/mL), followed by the derived AgNPs (67.99 µg/mL). Ethanolic *G. urbanum* rhizome extract and its derived AgNPs also demonstrated the highest performance in metal ion chelating and hydroxyl radical scavenging assays, highlighting a broad range of potential biological applications.

Author Contributions M.I. methodology, writing the manuscript; M.C. , H.C.E., R.C.M. biological tests, analysis of the results; B.A.F., S.L., P.A.D., N.C. – synthesis, optimization, physico-chemical characterization; C.A. , H.V.– conceptualization, supervision; H.M. , M.A. – review & editing.

Funding This research was funded by grant number 4712/25.02.2021, Young Researcher Grant, funded by Grigore T. Popa University of Medicine and Pharmacy, Iasi, Romania.

Data Availability No datasets were generated or analysed during the current study.

Declarations

Conflict of Interest The authors declare that the research was conducted without any commercial or financial relationships that could be construed as a potential conflict of interest.

Open Access This article is licensed under a Creative Commons Attribution 4.0 International License, which permits use, sharing, adaptation, distribution and reproduction in any medium or format, as long as you give appropriate credit to the original author(s) and the source, provide a link to the Creative Commons licence, and indicate if changes were made. The images or other third party material in this article are included in the article's Creative Commons licence, unless indicated otherwise in a credit line to the material. If material is not included in the article's Creative Commons licence and your intended use is not permitted by statutory regulation or exceeds the permitted use, you will need to obtain permission directly from the copyright holder. To view a copy of this licence, visit http://creativecommons.org/licenses/by/4.0/.

References

1. M.H. Siddique, B. Aslam, M. Imran, A. Ashraf, H. Nadeem, S. Hayat et al., Effect of silver nanoparticles on Biofilm formation and EPS production of Multidrug-Resistant < i > Klebsiella pneumoniae. Biomed. Res. Int. **2020**, 6398165 (2020). https://doi.org/10.1155/2020/6398165
2. P.R. More, S. Pandit, A.D. Filippis, G. Franci, I. Mijakovic, M. Galdiero, Silver nanoparticles: bactericidal and mechanistic Approach against Drug Resistant pathogens. Microorganisms. (2023). https://doi.org/10.3390/microorganisms11020369
3. C.J.L. Murray, K.S. Ikuta, F. Sharara, L. Swetschinski, G. Robles Aguilar, A. Gray et al., Global burden of bacterial antimicrobial resistance in 2019: a systematic analysis. Lancet. **399**(10325), 629–655 (2022). https://doi.org/10.1016/S0140-6736(21)02724-0
4. R.E. Nelson, K.M. Hatfield, H. Wolford, M.H. Samore, R.D. Scott, I.I. Reddy, National Estimates of Healthcare costs Associated with Multidrug-resistant bacterial infections among hospitalized patients in the United States. Clin. Infect. Dis. **72**(Supplement1), S17–S26 (2021). https://doi.org/10.1093/cid/ciaa1581
5. E.M. Mateo, M. Jiménez, Silver Nanoparticle-Based Therapy: Can It Be Useful to Combat Multi-Drug Resistant Bacteria? Antibiotics. 2022 https://doi.org/10.3390/antibiotics11091205
6. A. Chinnathambi, S.A. Alharbi, D. Joshi, V.S. Jhanani, G.K. On-uma, Synthesis of AgNPs from leaf extract of Naringi crenulata and evaluation of its antibacterial activity against multidrug resistant bacteria. Environ. Res. **216**, 114455 (2023). https://doi.org/10.1016/j.envres.2022.114455
7. T.D. Tavares, J.C. Antunes, J. Padrão, A.I. Ribeiro, A. Zille, M.T.P. Amorim et al., Activity of specialized biomolecules against gram-positive and gram-negative bacteria. Antibiotics. (2020). https://doi.org/10.3390/antibiotics9060314
8. V. Patil, S. Mahajan, M. Kulkarni, K. Patil, C. Rode, A. Coronas et al., Synthesis of silver nanoparticles colloids in imidazolium halide ionic liquids and their antibacterial activities for gram-positive and gram-negative bacteria. Chemosphere. **243**, 125302 (2020). https://doi.org/10.1016/j.chemosphere.2019.125302
9. R.A. Bapat, T.V. Chaubal, C.P. Joshi, P.R. Bapat, H. Choudhury, M. Pandey et al., An overview of application of silver nanoparticles

for biomaterials in dentistry. Mater. Sci. Engineering: C **91**, 881–898 (2018). https://doi.org/10.1016/j.msec.2018.05.069
10. A. Ahmed, M. Usman, Z. Ji, M. Rafiq, B. Yu, Y. Shen et al., Nature-inspired biogenic synthesis of silver nanoparticles for antibacterial applications. Mater. Today Chem. **27**, 101339 (2023). https://doi.org/10.1016/j.mtchem.2022.101339
11. A. Menichetti, A. Mavridi-Printezi, D. Mordini, M. Montalti, Effect of size, shape and surface functionalization on the antibacterial activity of silver nanoparticles. J. Funct. Biomaterials. (2023). https://doi.org/10.3390/jfb14050244
12. M. Wypij, T. Jędrzejewski, J. Trzcińska-Wencel, M. Ostrowski, M. Rai, P. Golińska, Green Synthesized Silver nanoparticles: Antibacterial and Anticancer activities, Biocompatibility, and analyses of surface-attached proteins. Front. Microbiol. 2021;**12**
13. K.N. Shashiraj, S. Nayaka, R.S. Kumar, G.B. Kantli, D.S. Basavarajappa, P.V. Gunagambhire et al., Rotheca Serrata Flower Bud Extract mediated Bio-friendly Preparation of Silver nanoparticles: their characterizations, Anticancer, and apoptosis inducing ability against pancreatic ductal Adenocarcinoma Cell line. Processes. (2023). https://doi.org/10.3390/pr11030893
14. H. Singh, J. Du, P. Singh, T.H. Yi, Ecofriendly synthesis of silver and gold nanoparticles by Euphrasia officinalis leaf extract and its biomedical applications. Artif. Cells Nanomed. Biotechnol. **46**(6), 1163–1170 (2018). https://doi.org/10.1080/21691401.2017.1362417
15. H.H. Math, K.N. Shashiraj, R.S. Kumar, M. Rudrappa, M.P. Bhat, D.S. Basavarajappa et al., Investigation of in vitro anticancer and apoptotic potential of Biofabricated Silver nanoparticles from Cardamine hirsuta (L.) Leaf Extract against Caco-2 cell line. Inorganics. (2023). https://doi.org/10.3390/inorganics11080322
16. S.K. Nagaraja, R.S. Kumar, B. Chakraborty, H. Hiremath, A.I. Almansour, K. Perumal et al., Biomimetic synthesis of silver nanoparticles using Cucumis sativus var. Hardwickii fruit extract and their characterizations, anticancer potential and apoptosis studies against Pa-1 (human ovarian teratocarcinoma) cell line via flow cytometry. Appl. Nanosci. **13**(4), 3073–3084 (2023). https://doi.org/10.1007/s13204-022-02386-w
17. P. Bélteky, A. Rónavári, D. Zakupszky, E. Boka, N. Igaz, B. Szerencsés et al., Are smaller nanoparticles always better? Understanding the Biological effect of size-dependent silver nanoparticle aggregation under Biorelevant conditions. Int. J. Nanomed. **16**(null), 3021–3040 (2021). https://doi.org/10.2147/IJN.S304138
18. A.S. Joshi, P. Singh, I. Mijakovic, Interactions of gold and silver nanoparticles with bacterial biofilms: molecular interactions behind inhibition and resistance. Int. J. Mol. Sci. (2020). https://doi.org/10.3390/ijms21207658
19. X. Gu, Z. Xu, L. Gu, H. Xu, F. Han, B. Chen et al., Preparation and antibacterial properties of gold nanoparticles: a review. Environ. Chem. Lett. **19**(1), 167–187 (2021). https://doi.org/10.1007/s10311-020-01071-0
20. B. Ramalingam, T. Parandhaman, S.K. Das, Antibacterial effects of Biosynthesized Silver nanoparticles on Surface Ultrastructure and Nanomechanical properties of Gram-negative Bacteria viz. Escherichia coli and Pseudomonas aeruginosa. ACS Appl. Mater. Interfaces. **8**(7), 4963–4976 (2016). https://doi.org/10.1021/acsami.6b00161
21. M.M. Rohde, C.M. Snyder, J. Sloop, S.R. Solst, G.L. Donati, D.R. Spitz et al., The mechanism of cell death induced by silver nanoparticles is distinct from silver cations. Part. Fibre Toxicol. **18**(1), 37 (2021). https://doi.org/10.1186/s12989-021-00430-1
22. E.O. Mikhailova, Silver nanoparticles: mechanism of action and probable Bio-application. J. Funct. Biomaterials. (2020). https://doi.org/10.3390/jfb11040084
23. V. Pareek, A. Bhargava, R. Gupta, N. Jain, J. Panwar, Synthesis and applications of Noble Metal nanoparticles: a review. Adv. Sci. Eng. Med. **9**(7), 527–544 (2017). https://doi.org/10.1166/asem.2017.2027
24. D. Garg, A. Sarkar, P. Chand, P. Bansal, D. Gola, S. Sharma et al., Synthesis of silver nanoparticles utilizing various biological systems: mechanisms and applications—a review. Prog. Biomater. **9**(3), 81–95 (2020). https://doi.org/10.1007/s40204-020-00135-2
25. M. Naghmachi, A. Raissi, P. Baziyar, F. Homayoonfar, F. Amirmahani, M. Danaei, Green synthesis of silver nanoparticles (AgNPs) by Pistacia terebinthus extract: Comprehensive evaluation of antimicrobial, antioxidant and anticancer effects. Biochem. Biophys. Res. Commun. **608**, 163–169 (2022). https://doi.org/10.1016/j.bbrc.2022.04.003
26. M. Hosny, M. Fawzy, Y.A. El-Badry, E.E. Hussein, A.S. Eltaweil, Plant-assisted synthesis of gold nanoparticles for photocatalytic, anticancer, and antioxidant applications. J. Saudi Chem. Soc. **26**(2), 101419 (2022). https://doi.org/10.1016/j.jscs.2022.101419
27. J. Venkatesan, J.-Y. Lee, D.S. Kang, S. Anil, S.-K. Kim, M.S. Shim et al., Antimicrobial and anticancer activities of porous chitosan-alginate biosynthesized silver nanoparticles. Int. J. Biol. Macromol. **98**, 515–525 (2017). https://doi.org/10.1016/j.ijbiomac.2017.01.120
28. K. Venugopal, H. Ahmad, E. Manikandan, K. Thanigai Arul, K. Kavitha, M.K. Moodley et al., The impact of anticancer activity upon Beta vulgaris extract mediated biosynthesized silver nanoparticles (ag-NPs) against human breast (MCF-7), lung (A549) and pharynx (Hep-2) cancer cell lines. J. Photochem. Photobiol., B **173**, 99–107 (2017). https://doi.org/10.1016/j.jphotobiol.2017.05.031
29. J.R. Nakkala, R. Mata, S.R. Sadras, Green synthesized nano silver: synthesis, physicochemical profiling, antibacterial, anticancer activities and biological in vivo toxicity. J. Colloid Interface Sci. **499**, 33–45 (2017). https://doi.org/10.1016/j.jcis.2017.03.090
30. R. Vijayan, S. Joseph, B. Mathew, Indigofera tinctoria leaf extract mediated green synthesis of silver and gold nanoparticles and assessment of their anticancer, antimicrobial, antioxidant and catalytic properties. Artif. Cells Nanomed. Biotechnol. **46**(4), 861–871 (2018). https://doi.org/10.1080/21691401.2017.1345930
31. P.V. Subramanian, M.S. AlSalhi, S. Devanesan, P.A. Thomas, Evaluation of antioxidant, anticancer and DNA binding potentials of Noble Metal nanoparticles synthesized using Aristolochia indica and Indigofera tinctoria. J. Cluster Sci. **32**(4), 917–927 (2021). https://doi.org/10.1007/s10876-020-01858-9
32. R. Wang, X. Xu, A.M. Puja, H. Perumalsamy, S.R. Balusamy, H. Kim et al., Gold nanoparticles prepared with Phyllanthus emblica Fruit Extract and Bifidobacterium animalis subsp. lactis can induce apoptosis via mitochondrial impairment with inhibition of Autophagy in the human gastric Carcinoma Cell Line AGS. Nanomaterials. (2021). https://doi.org/10.3390/nano11051260
33. M. Chelly, S. Chelly, R. Zribi, H. Bouaziz-Ketata, R. Gdoura, N. Lavanya et al., Synthesis of silver and gold nanoparticles from Rumex Roseus Plant Extract and their application in Electrochemical sensors. Nanomaterials. (2021). https://doi.org/10.3390/nano11030739
34. M. Sharma, P. Monika, Thakur, R.V. Saini, R. Kumar, E. Torino, Unveiling antimicrobial and anticancerous behavior of AuNPs and AgNPs moderated by rhizome extracts of Curcuma longa from diverse altitudes of Himalaya. Sci. Rep. **10**(1), 10934 (2020). https://doi.org/10.1038/s41598-020-67673-4
35. D. Wang, J. Markus, C. Wang, Y.-J. Kim, R. Mathiyalagan, V.C. Aceituno et al., Green synthesis of gold and silver nanoparticles using aqueous extract of Cibotium barometz root. Artif. Cells Nanomed. Biotechnol. **45**(8), 1548–1555 (2017). https://doi.org/10.1080/21691401.2016.1260580
36. S. Basumatary, J. Daimari, A. Ghosh, A.K. Deka, Green synthesis of NPs (ag & au) from some plant families (Phyllanthaceae,

Lamiaceae, Rutaceae and Euphorbiaceae) and their application in therapeutics: a review. South. Afr. J. Bot. **166**, 624–635 (2024). https://doi.org/10.1016/j.sajb.2024.02.003
37. H.A. Ghramh, K.A. Khan, E.H. Ibrahim, W.N. Setzer, Synthesis of gold nanoparticles (AuNPs) using Ricinus communis Leaf ethanol extract, their characterization, and Biological Applications. Nanomaterials. (2019). https://doi.org/10.3390/nano9050765
38. M. Bunse, L.K. Mailänder, P. Lorenz, F.C. Stintzing, D.R. Kammerer, Evaluation of Geum urbanum L. extracts with respect to their antimicrobial potential. Chem. Biodivers. **19**(2), e202100850 (2022). https://doi.org/10.1002/cbdv.202100850
39. Q. Ton That, T.V. Nguyen Thien, H.P. Dang, Le N. Hoan, L.K.T. Vo, M.H.D. Nguyen et al., Chemical constituents of Geum urbanum L. roots. Nat. Prod. Res. **32**(21), 2529–2534 (2018). https://doi.org/10.1080/14786419.2018.1425844
40. M. Bunse, P. Lorenz, F.C. Stintzing, D.R. Kammerer, Insight into the secondary metabolites of Geum urbanum L. and Geum rivale L. Seeds (Rosaceae). Plants. (2021). https://doi.org/10.3390/plants10061219
41. V. Neshati, S. Mollazadeh, B.S. Fazly Bazzaz, M. Iranshahi, M. Mojarrad, H. Naderi-Meshkin et al., Cardiogenic effects of characterized Geum urbanum extracts on adipose-derived human mesenchymal stem cells. Biochem. Cell Biol. **96**(5), 610–618 (2018). https://doi.org/10.1139/bcb-2017-0313
42. S. Granica, A. Kłębowska, M. Kosiński, J.P. Piwowarski, M.K. Dudek, S. Kaźmierski et al., Effects of Geum urbanum L. root extracts and its constituents on polymorphonuclear leucocytes functions. Significance in periodontal diseases. J. Ethnopharmacol. **188**, 1–12 (2016). https://doi.org/10.1016/j.jep.2016.04.030
43. A.E. Al-Snafi, Constituents and pharmacology of Geum urbanum-A review. IOSR J. Pharm. **9**(5), 28–33 (2019)
44. L. Dimitrova, M.M. Zaharieva, M. Popova, N. Kostadinova, I. Tsvetkova, V. Bankova et al., Antimicrobial and antioxidant potential of different solvent extracts of the medicinal plant Geum urbanum L. Chem. Cent. J. **11**(1), 113 (2017). https://doi.org/10.1186/s13065-017-0343-8
45. M.M. Zaharieva, L.L. Dimitrova, S. Philipov, I. Nikolova, N. Vilhelmova, P. Grozdanov et al., In Vitro Antineoplastic and antiviral activity and in vivo toxicity of Geum urbanum L. extracts. Molecules. (2022). https://doi.org/10.3390/molecules27010245
46. A. Farzaneh, M.A. Faramarzi, M.R. Delnavazi, H.R. Monsef-Esfahani, H.R. Adhami*, In Vitro anti-diabetic and anti-oxidant activities of Geum species from Iran. Res. J. Pharmacognosy. **9**(2), 37–44 (2022). https://doi.org/10.22127/rjp.2021.304041.1788
47. M. Szymanski, R. Dobrucka, Evaluation of Phytotoxicity of Bimetallic Ag/Au nanoparticles synthesized using Geum urbanum L. J. Inorg. Organomet. Polym Mater. **31**(6), 2459–2470 (2021). https://doi.org/10.1007/s10904-020-01814-0
48. I. Macovei, S.V. Luca, K. Skalicka-Woźniak, L. Sacarescu, P. Pascariu, A. Ghilan et al., Phyto-functionalized silver nanoparticles derived from Conifer Bark extracts and evaluation of their Antimicrobial and Cytogenotoxic effects. Molecules. (2022). https://doi.org/10.3390/molecules27010217
49. I. Macovei, S.V. Luca, K. Skalicka-Woźniak, C.E. Horhogea, C.M. Rimbu, L. Sacarescu et al., Silver nanoparticles synthesized from Abies alba and Pinus sylvestris bark extracts: characterization, antioxidant, cytotoxic, and Antibacterial effects. Antioxidants. (2023). https://doi.org/10.3390/antiox12040797
50. S.K. Chandraker, M. Lal, P. Dhruve, R.P. Singh, R. Shukla, D.N.A. Cytotoxic, Antimitotic, Binding, Photocatalytic, H2O2 sensing, and antioxidant properties of Biofabricated Silver nanoparticles using Leaf Extract of Bryophyllum pinnatum (Lam.) Oken. Front. Mol. Biosci. 2021;**7**
51. S. Satpathy, A. Patra, B. Ahirwar, M.D. Hussain, Process optimization for green synthesis of gold nanoparticles mediated by extract of Hygrophila Spinosa T. Anders and their biological applications. Phys. E: Low-dimensional Syst. Nanostruct. **121**, 113830 (2020). https://doi.org/10.1016/j.physe.2019.113830
52. M. Younas, M.H. Rasool, M. Khurshid, A. Khan, M.Z. Nawaz, I. Ahmad et al., Moringa oleifera leaf extract mediated green synthesis of silver nanoparticles and their antibacterial effect against selected gram-negative strains. Biochem. Syst. Ecol. **107**, 104605 (2023). https://doi.org/10.1016/j.bse.2023.104605
53. A. Bharali, H. Sarma, N. Biswas, J.M. Kalita, B. Das, B.P. Sahu et al., Green synthesis of silver nanoparticles using hydroalcoholic root extract of Potentilla fulgens and evaluation of its cutaneous wound healing potential. Mater. Today Commun. **35**, 106050 (2023). https://doi.org/10.1016/j.mtcomm.2023.106050
54. S. Malik, M. Niazi, M. Khan, B. Rauff, S. Anwar, F. Amin et al., Cytotoxicity study of gold nanoparticle synthesis using Aloe vera, Honey, and Gymnema sylvestre Leaf Extract. ACS Omega. **8**(7), 6325–6336 (2023). https://doi.org/10.1021/acsomega.2c06491
55. W. Handayani, A.S. Ningrum, C. Imawan, The Role of pH in Synthesis Silver Nanoparticles Using Pometia pinnata (Matoa) Leaves Extract as Bioreductor. Journal of Physics: Conference Series. 2020;1428(1):012021. https://doi.org/10.1088/1742-6596/1428/1/012021
56. D. Tripathi, A. Modi, G. Narayan, S.P. Rai, Green and cost effective synthesis of silver nanoparticles from endangered medicinal plant Withania coagulans and their potential biomedical properties. Mater. Sci. Engineering: C **100**, 152–164 (2019). https://doi.org/10.1016/j.msec.2019.02.113
57. T.C.P. Dinis, V.M.C. Madeira, L.M. Almeida, Action of phenolic derivatives (Acetaminophen, Salicylate, and 5-Aminosalicylate) as inhibitors of membrane lipid peroxidation and as Peroxyl Radical scavengers. Arch. Biochem. Biophys. **315**(1), 161–169 (1994). https://doi.org/10.1006/abbi.1994.1485
58. S. Éverton da Silva, T. Leticia de Melo, C. Juliana Cristina, M. Laura Paulino, José Rivaldo dos S, G. José Eduardo et al., An analytical method for the quantitative determination of iron ion chelating capacity: development and validation. Acta Scientiarum Biological Sciences. 2022;44(1). https://doi.org/10.4025/actascibiolsci.v44i1.59739
59. J.B. Jeong, S. Chul Hong, H. Jin Jeong, 3,4-Dihydroxybenzaldehyde purified from the barley seeds (Hordeum vulgare) inhibits oxidative DNA damage and apoptosis via its antioxidant activity. Phytomedicine. **16**(1), 85–94 (2009). https://doi.org/10.1016/j.phymed.2008.09.013
60. A. Zuorro, A. Iannone, S. Natali, R. Lavecchia, Green Synthesis of Silver Nanoparticles Using Bilberry and Red Currant Waste extracts. Processes. (2019). https://doi.org/10.3390/pr7040193
61. L. Biao, S. Tan, X. Zhang, J. Gao, Z. Liu, Y. Fu, Synthesis and characterization of proanthocyanidins-functionalized ag nanoparticles. Colloids Surf., B **169**, 438–443 (2018). https://doi.org/10.1016/j.colsurfb.2018.05.050
62. M.A. Sobi, D. Usha, R. Rajagopal, S. Arokiyaraj, M.R. Bindhu, Phytosynthesizing gold nanoparticles: characterization, bioactivity, and catalysis evaluation. J. Mol. Struct. **1302**, 137308 (2024). https://doi.org/10.1016/j.molstruc.2023.137308
63. J. Oszmianski, A. Wojdylo, E. Lamer-Zarawska, K. Swiader, Antioxidant tannins from Rosaceae plant roots. Food Chem. **100**(2), 579–583 (2007). https://doi.org/10.1016/j.foodchem.2005.09.086
64. L. Panizzi, S. Catalano, C. Miarelli, P.L. Cioni, E. Campeol, In vitro antimicrobial activity of extracts and isolated constituents of Geum rivale. Phytother. Res. **14**(7), 561–563 (2000). https://doi.org/10.1002/1099-1573(200011)14:7%3C561::AID-PTR651%3E3.0.CO;2-H
65. R. Kumar, S.M. Roopan, A. Prabhakarn, V.G. Khanna, S. Chakroborty, Agricultural waste Annona squamosa peel extract: biosynthesis of silver nanoparticles. Spectrochim. Acta Part A Mol. Biomol. Spectrosc. **90**, 173–176 (2012). https://doi.org/10.1016/j.saa.2012.01.029

66. Z.--R. Mashwani, T. Khan, M.A. Khan, A. Nadhman, Synthesis in plants and plant extracts of silver nanoparticles with potent antimicrobial properties: current status and future prospects. Appl. Microbiol. Biotechnol. **99**(23), 9923–9934 (2015). https://doi.org/10.1007/s00253-015-6987-1
67. M. Tesfaye, Y. Gonfa, G. Tadesse, T. Temesgen, S. Periyasamy, Green synthesis of silver nanoparticles using Vernonia amygdalina plant extract and its antimicrobial activities. Heliyon. **9**(6), e17356 (2023). https://doi.org/10.1016/j.heliyon.2023.e17356
68. B. Tessema, G. Gonfa, S.M. Hailegiorgis, S.V. Prabhu, S. Manivannan, Synthesis and characterization of silver nanoparticles using reducing agents of bitter leaf (Vernonia amygdalina) extract and tri-sodium citrate. Nano-Structures Nano-Objects. **35**, 100983 (2023). https://doi.org/10.1016/j.nanoso.2023.100983
69. A.L. Toppo, S. Dhagat, S. Eswari Jujjavarapu, Comparative study of response surface methodology and artificial neural network for optimization of process parameters for synthesis of gold nanoparticles by Desmostachya bipinnata extract. Prep. Biochem. Biotechnol. **53**(2), 195–206 (2023). https://doi.org/10.1080/10826068.2022.2062773
70. D. Diksha, S.K. Gupta, P. Gupta, U.C. Banerjee, D. Kalita, Antibacterial potential of gold nanoparticles synthesized from Leaf Extract of Syzygium cumini against Multidrug-resistant urinary tract pathogens. Cureus. **15**(2), e34830 (2023). https://doi.org/10.7759/cureus.34830
71. A. Salayová, Z. Bedlovičová, N. Daneu, M. Baláž, Z. Lukáčová Bujňáková, Ľ. Balážová et al., Green Synthesis of Silver Nanoparticles with antibacterial activity using various Medicinal Plant extracts: morphology and Antibacterial Efficacy. Nanomaterials. (2021). https://doi.org/10.3390/nano11041005
72. Y. Zhang, X. Cheng, Y. Zhang, X. Xue, Y. Fu, Biosynthesis of silver nanoparticles at room temperature using aqueous aloe leaf extract and antibacterial properties. Colloids Surf., a **423**, 63–68 (2013). https://doi.org/10.1016/j.colsurfa.2013.01.059
73. R. Seifipour, M. Nozari, L. Pishkar, Green Synthesis of Silver Nanoparticles using Tragopogon Collinus Leaf Extract and Study of their Antibacterial effects. J. Inorg. Organomet. Polym Mater. **30**(8), 2926–2936 (2020). https://doi.org/10.1007/s10904-020-01441-9
74. A.A. Subhani, M. Irshad, S. Ali, M. Jawad, M.F. Akhtar, M. Summer, UV-spectrophotometric optimization of temperature, pH, concentration and Time for Eucalyptus Globulus Capped Silver Nanoparticles Synthesis, their characterization and evaluation of Biological Applications. J. Fluoresc. **34**(2), 655–666 (2024). https://doi.org/10.1007/s10895-023-03260-w
75. S.N.H. Azmi, B.M.H. Al-Jassasi, H.M.S. Al-Sawafi, S.H.G. Al-Shukaili, N. Rahman, M. Nasir, Optimization for synthesis of silver nanoparticles through response surface methodology using leaf extract of Boswellia sacra and its application in antimicrobial activity. Environ. Monit. Assess. **193**(8), 497 (2021). https://doi.org/10.1007/s10661-021-09301-w
76. B. Ahmad, J. Ali, S. Bashir, Optimization and effects of different reaction conditions for the bioinspired synthesis of silver nanoparticles using Hippophae rhamnoides Linn. Leaves aqueous extract. World Appl. Sci. J. **22**, 836–843 (2013)
77. D. Susanthy, S.J. Santosa, E.S. Kunarti, The Synthesis and Stability Study of Silver Nanoparticles Prepared by Using p -Aminobenzoic Acid as Reducing and Stabilizing Agent. Indonesian Journal of Chemistry; Vol 18, No 3 (2018). 2018. https://doi.org/10.22146/ijc.29312
78. H.M.M. Ibrahim, Green synthesis and characterization of silver nanoparticles using banana peel extract and their antimicrobial activity against representative microorganisms. J. Radiation Res. Appl. Sci. **8**(3), 265–275 (2015). https://doi.org/10.1016/j.jrras.2015.01.007
79. I. Ahamad, N. Aziz, A. Zaki, T. Fatma, Synthesis and characterization of silver nanoparticles using Anabaena variabilis as a potential antimicrobial agent. J. Appl. Phycol. **33**(2), 829–841 (2021). https://doi.org/10.1007/s10811-020-02323-w
80. V.R. Netala, V.S. Kotakadi, P. Bobbu, S.A. Gaddam, V. Tartte, Endophytic fungal isolate mediated biosynthesis of silver nanoparticles and their free radical scavenging activity and anti microbial studies. 3 Biotech. **6**(2), 132 (2016). https://doi.org/10.1007/s13205-016-0433-7
81. B. Bahrami-Teimoori, Y. Nikparast, M. Hojatianfar, M. Akhlaghi, R. Ghorbani, H.R. Pourianfar, Characterisation and antifungal activity of silver nanoparticles biologically synthesised by Amaranthus retroflexus leaf extract. J. Exp. Nanosci. **12**(1), 129–139 (2017). https://doi.org/10.1080/17458080.2017.1279355
82. L. Ma, W. Su, J.-X. Liu, X.-X. Zeng, Z. Huang, W. Li et al., Optimization for extracellular biosynthesis of silver nanoparticles by Penicillium Aculeatum Su1 and their antimicrobial activity and cytotoxic effect compared with silver ions. Mater. Sci. Engineering: C **77**, 963–971 (2017). https://doi.org/10.1016/j.msec.2017.03.294
83. A. Turki, El A. Oudiani, S. Msahli, F. Sakli, Investigation of OH bond energy for chemically treated alfa fibers. Carbohydr. Polym. **186**, 226–235 (2018). https://doi.org/10.1016/j.carbpol.2018.01.030
84. R. Vijayabharathi, A. Sathya, S. Gopalakrishnan, Extracellular biosynthesis of silver nanoparticles using Streptomyces griseoplanus SAI-25 and its antifungal activity against Macrophomina Phaseolina, the charcoal rot pathogen of sorghum. Biocatal. Agric. Biotechnol. **14**, 166–171 (2018). https://doi.org/10.1016/j.bcab.2018.03.006
85. S. Pallavi, S. Rudayni, H.A. Bepari, A. Niazi, S.K. Nayaka, Green synthesis of silver nanoparticles using Streptomyces hirsutus strain SNPGA-8 and their characterization, antimicrobial activity, and anticancer activity against human lung carcinoma cell line A549. Saudi J. Biol. Sci. **29**(1), 228–238 (2022). https://doi.org/10.1016/j.sjbs.2021.08.084
86. M. Das, A. Mondal, K. Patowary, H. Malipeddi, Biosynthesis of AgNPs using aqueous leaf extract of Ipomoea eriocarpa and their anti-inflammatory effect on carrageenan-induced paw edema in male Wistar rats. IET Nanobiotechnol. **11**(3), 225–229 (2017). https://doi.org/10.1049/iet-nbt.2016.0034
87. Y.S. Pontaza-Licona, A.L. Ramos-Jacques, J.A. Cervantes-Chavez, J.L. López-Miranda, J. Ruíz-Baltazar ÁdJ, Maya-Cornejo et al., Alcoholic extracts from Paulownia tomentosa leaves for silver nanoparticles synthesis. Results Phys. **12**, 1670–1679 (2019). https://doi.org/10.1016/j.rinp.2019.01.082
88. M. Adoni, M. Yadam, S.A. Gaddam, U. Rayalacheruvu, V.S. Kotakadi, Antimicrobial, antioxidant, and dye degradation properties of biosynthesized silver nanoparticles from Artemisia annua L. Lett. Appl. Nanobiosci. **10**, 1981–1992 (2020)
89. G.C. Acharya, N. Ponnam, M. Kumari, T.K. Roy, K.S. Shivashankara, M.R. Sahoo, Phytochemical profiling of spiny coriander (Eryngium foetidum L.)–A potential perennial spicing-culinary herb of eastern India. Acta Chromatographica. **34**(2), 197–202 (2021)
90. J.M. Moreno-Vargas, L.M. Echeverry-Cardona, L.E. Moreno-Montoya, E. Restrepo-Parra, Evaluation of antifungal activity of Ag nanoparticles synthetized by Green Chemistry against Fusarium solani and Rhizopus stolonifera. Nanomaterials. (2023). https://doi.org/10.3390/nano13030548
91. P.K. Tyagi, S. Tyagi, D. Gola, A. Arya, S.A. Ayatollahi, M.M. Alshehri et al., Ascorbic acid and polyphenols mediated Green synthesis of silver nanoparticles from <i>Tagetes erecta L. Aqueous Leaf Extract and Studied their antioxidant Properties. J. Nanomaterials. **2021**, 6515419 (2021). https://doi.org/10.1155/2021/6515419

92. M.A. Elbahnasawy, A.M. Shehabeldine, A.M. Khattab, B.H. Amin, A.H. Hashem, Green biosynthesis of silver nanoparticles using novel endophytic Rothia Endophytica: characterization and anticandidal activity. J. Drug Deliv. Sci. Technol. **62**, 102401 (2021). https://doi.org/10.1016/j.jddst.2021.102401
93. T. Dutta, S.K. Chowdhury, N.N. Ghosh, A.P. Chattopadhyay, M. Das, V. Mandal, Green synthesis of antimicrobial silver nanoparticles using fruit extract of Glycosmis pentaphylla and its theoretical explanations. J. Mol. Struct. **1247**, 131361 (2022). https://doi.org/10.1016/j.molstruc.2021.131361
94. S.S. Jaffar, S. Saallah, M. Misson, S. Siddiquee, J. Roslan, W. Lenggoro, Green synthesis of flower-Like carrageenan-silver nanoparticles and elucidation of its physicochemical and Antibacterial properties. Molecules. (2023). https://doi.org/10.3390/molecules28020907
95. S. Ghojavand, M. Madani, J. Karimi, Green Synthesis, characterization and antifungal activity of silver nanoparticles using stems and flowers of Felty Germander. J. Inorg. Organomet. Polym Mater. **30**(8), 2987–2997 (2020). https://doi.org/10.1007/s10904-020-01449-1
96. S. Poopathi, De L.J. Britto, V.L. Praba, C. Mani, M. Praveen, Synthesis of silver nanoparticles from Azadirachta indica—a most effective method for mosquito control. Environ. Sci. Pollut. Res. **22**(4), 2956–2963 (2015). https://doi.org/10.1007/s11356-014-3560-x
97. S. Rasool, M.A. Raza, F. Manzoor, Z. Kanwal, S. Riaz, M.J. Iqbal et al., Biosynthesis, characterization and anti-dengue vector activity of silver nanoparticles prepared from Azadirachta indica and Citrullus colocynthis. Royal Soc. Open. Sci. **7**(9), 200540 (2020). https://doi.org/10.1098/rsos.200540
98. Y. He, F. Wei, Z. Ma, H. Zhang, Q. Yang, B. Yao et al., Green synthesis of silver nanoparticles using seed extract of Alpinia katsumadai, and their antioxidant, cytotoxicity, and antibacterial activities. RSC Adv. **7**(63), 39842–39851 (2017)
99. M.G. Heinemann, C.H. Rosa, G.R. Rosa, D. Dias, Biogenic synthesis of gold and silver nanoparticles used in environmental applications: a review. Trends Environ. Anal. Chem. **30**, e00129 (2021). https://doi.org/10.1016/j.teac.2021.e00129
100. A. Abdelmoteleb, B. Valdez-Salas, M. Carrillo-Beltran, D.D. Hernandez, D. González-Mendoza, Green synthesis of silver nanoparticles using Pluchea sericea a native plants from Baja California, Mexico and their potential application as antimicrobials. Iran. J. Sci. Technol. Trans. A: Sci. **42**(2), 457–463 (2018). https://doi.org/10.1007/s40995-016-0019-6
101. S. Bhattacharjee, DLS and Zeta potential – what they are and what they are not? J. Controlled Release. **235**, 337–351 (2016). https://doi.org/10.1016/j.jconrel.2016.06.017
102. R.C. Murdock, L. Braydich-Stolle, A.M. Schrand, J.J. Schlager, S.M. Hussain, Characterization of Nanomaterial Dispersion in Solution prior to in vitro exposure using dynamic light scattering technique. Toxicol. Sci. **101**(2), 239–253 (2008). https://doi.org/10.1093/toxsci/kfm240
103. T.R. Santiago, C.C. Bonatto, M. Rossato, C.A.P. Lopes, C.A. Lopes, G. Mizubuti, Green synthesis of silver nanoparticles using tomato leaf extract and their entrapment in chitosan nanoparticles to control bacterial wilt. J. Sci. Food. Agric. **99**(9), 4248–4259 (2019). https://doi.org/10.1002/jsfa.9656
104. A. Shahzad, H. Saeed, M. Iqtedar, S.Z. Hussain, A. Kaleem, R. Abdullah et al., Size-controlled production of silver nanoparticles by <i>aspergillus fumigatus BTCB10: likely antibacterial and cytotoxic effects. J. Nanomaterials. **2019**, 5168698 (2019). https://doi.org/10.1155/2019/5168698
105. S. Coseri, A. Spatareanu, L. Sacarescu, C. Rimbu, D. Suteu, S. Spirk et al., Green synthesis of the silver nanoparticles mediated by pullulan and 6-carboxypullulan. Carbohydr. Polym. **116**, 9–17 (2015). https://doi.org/10.1016/j.carbpol.2014.06.008
106. Z. Heidari, A. Salehzadeh, S.A. Sadat Shandiz, S. Tajdoost, Anti-cancer and anti-oxidant properties of ethanolic leaf extract of Thymus vulgaris and its bio-functionalized silver nanoparticles. 3 Biotech. **8**(3), 177 (2018). https://doi.org/10.1007/s13205-018-1199-x
107. K.B. Narayanan, H.H. Park, Antifungal activity of silver nanoparticles synthesized using turnip leaf extract (Brassica rapa L.) against wood rotting pathogens. Eur. J. Plant Pathol. **140**(2), 185–192 (2014). https://doi.org/10.1007/s10658-014-0399-4
108. S. Poadang, N. Yongvanich, S. Phongtongpasuk, Synthesis, characterization, and antibacterial properties of silver nanoparticles prepared from aqueous peel extract of pineapple, ananas comosus. Chiang Mai Univ. J. Nat. Sci. **16**(2), 123–133 (2017)
109. P. Chirumamilla, S.B. Dharavath, S. Taduri, Eco-friendly green synthesis of silver nanoparticles from Leaf Extract of Solanum khasianum: Optical properties and Biological Applications. Appl. Biochem. Biotechnol. **195**(1), 353–368 (2023). https://doi.org/10.1007/s12010-022-04156-4
110. T.S. Alomar, N. AlMasoud, M.A. Awad, M.F. El-Tohamy, D.A. Soliman, An eco-friendly plant-mediated synthesis of silver nanoparticles: characterization, pharmaceutical and biomedical applications. Mater. Chem. Phys. **249**, 123007 (2020). https://doi.org/10.1016/j.matchemphys.2020.123007
111. S.A. Bhat, N. Rashid, M.A. Rather, S.A. Pandit, G.M. Rather, P.P. Ingole et al., PdAg Bimetallic Nanoalloy-decorated graphene: a nanohybrid with unprecedented Electrocatalytic, Catalytic, and sensing activities. ACS Appl. Mater. Interfaces. **10**(19), 16376–16389 (2018). https://doi.org/10.1021/acsami.8b00510
112. R. Kumari, R.C. Mishra, R. Sheoran, J.P. Yadav, Fractionation of antimicrobial compounds from Acacia nilotica twig extract against oral pathogens. Biointerface Res. Appl. Chem. **10**, 7097–7105 (2020)
113. A. Jain, F. Ahmad, D. Gola, A. Malik, N. Chauhan, P. Dey et al., Multi dye degradation and antibacterial potential of papaya leaf derived silver nanoparticles. Environ. Nanatechnol. Monit. Manage. **14**, 100337 (2020). https://doi.org/10.1016/j.enmm.2020.100337
114. F. Jalilian, A. Chahardoli, K. Sadrjavadi, A. Fattahi, Y. Shokoohinia, Green synthesized silver nanoparticle from Allium ampeloprasum aqueous extract: characterization, antioxidant activities, antibacterial and cytotoxicity effects. Adv. Powder Technol. **31**(3), 1323–1332 (2020). https://doi.org/10.1016/j.apt.2020.01.011
115. A. Roy, O. Bulut, S. Some, A.K. Mandal, M.D. Yilmaz, Green synthesis of silver nanoparticles: biomolecule-nanoparticle organizations targeting antimicrobial activity. RSC Adv. **9**(5), 2673–2702 (2019)
116. C. Vanlalveni, S. Lallianrawna, A. Biswas, M. Selvaraj, B. Changmai, S.L. Rokhum, Green synthesis of silver nanoparticles using plant extracts and their antimicrobial activities: a review of recent literature. RSC Adv. **11**(5), 2804–2837 (2021)
117. K. Gopinath, S. Kumaraguru, K. Bhakyaraj, S. Mohan, K.S. Venkatesh, M. Esakkirajan et al., Green synthesis of silver, gold and silver/gold bimetallic nanoparticles using the Gloriosa superba leaf extract and their antibacterial and antibiofilm activities. Microb. Pathog. **101**, 1–11 (2016). https://doi.org/10.1016/j.micpath.2016.10.011
118. S.A. Khan, S. Shahid, C.-S. Lee, Green Synthesis of Gold and silver nanoparticles using Leaf Extract of Clerodendrum inerme; characterization, Antimicrobial, and antioxidant activities. Biomolecules. (2020). https://doi.org/10.3390/biom10060835
119. M. Kumari, S. Pandey, V.P. Giri, A. Bhattacharya, R. Shukla, A. Mishra et al., Tailoring shape and size of biogenic silver nanoparticles to enhance antimicrobial efficacy against MDR bacteria. Microb. Pathog. **105**, 346–355 (2017). https://doi.org/10.1016/j.micpath.2016.11.012

120. M. Gao, L. Sun, Z. Wang, Y. Zhao, Controlled synthesis of Ag nanoparticles with different morphologies and their antibacterial properties. Mater. Sci. Engineering: C **33**(1), 397–404 (2013). https://doi.org/10.1016/j.msec.2012.09.005
121. H. Ghaffari, B.J. Ghassam, H. Prakash, Evaluation of antioxidant and antiinflammatory activity of Stachys Lavandulifolia. Int. J. Pharm. Pharm. Sci. **4**(3), 691–696 (2012)
122. R. Punampalam, K.S. Khoo, N.W. Sit, Evaluation of antioxidant properties of phycobiliproteins and phenolic compounds extracted from Bangia atropurpurea. Malays J. Fundam Appl. Sci. **14**(2), 289–297 (2018)
123. S. Phongpaichit, J. Nikom, N. Rungjindamai, J. Sakayaroj, N. Hutadilok-Towatana, V. Rukachaisirikul et al., Biological activities of extracts from endophytic fungi isolated from Garcinia plants. FEMS Immunol. Med. Microbiol. **51**(3), 517–525 (2007). https://doi.org/10.1111/j.1574-695X.2007.00331.x
124. H. Meng, Z. Dai, W. Zhang, Y. Liu, L. Lai, Molecular mechanism of 15-lipoxygenase allosteric activation and inhibition. Phys. Chem. Chem. Phys. **20**(21), 14785–14795 (2018). https://doi.org/10.1039/C7CP08586A
125. M. Lončarić, I. Strelec, T. Moslavac, D. Šubarić, V. Pavić, M. Molnar, Lipoxygenase inhibition by plant extracts. Biomolecules. (2021). https://doi.org/10.3390/biom11020152
126. S. Chen, H. Zou, Lipoxygenase Metabolism: critical pathways in Microglia-mediated Neuroinflammation and Neurodevelopmental disorders. Neurochem. Res. **47**(11), 3213–3220 (2022). https://doi.org/10.1007/s11064-022-03645-6
127. M. Govindappa, H. Farheen, C.P. Chandrappa, R.V. Channabasava, Rai, V.B. Raghavendra, Mycosynthesis of silver nanoparticles using extract of endophytic fungi, Penicillium species of Glycosmis mauritiana, and its antioxidant, antimicrobial, anti-inflammatory and tyrokinase inhibitory activity. Adv. Nat. Sci. NanoSci. NanoTechnol. **7**(3), 035014 (2016). https://doi.org/10.1088/2043-6262/7/3/035014
128. M. Govindappa, B. Hemashekhar, M.-K. Arthikala, V. Ravishankar Rai, Y.L. Ramachandra, Characterization, antibacterial, antioxidant, antidiabetic, anti-inflammatory and antityrosinase activity of green synthesized silver nanoparticles using Calophyllum tomentosum leaves extract. Results Phys. **9**, 400–408 (2018). https://doi.org/10.1016/j.rinp.2018.02.049
129. F. Khuda, Z. Ul Haq, I. Ilahi, R. Ullah, A. Khan, H. Fouad et al., Synthesis of gold nanoparticles using Sambucus Wightiana extract and investigation of its antimicrobial, anti-inflammatory, antioxidant and analgesic activities. Arab. J. Chem. **14**(10), 103343 (2021). https://doi.org/10.1016/j.arabjc.2021.103343
130. G. Das, J.K. Patra, H.-S. Shin, Biosynthesis, and potential effect of fern mediated biocompatible silver nanoparticles by cytotoxicity, antidiabetic, antioxidant and antibacterial, studies. Mater. Sci. Engineering: C **114**, 111011 (2020). https://doi.org/10.1016/j.msec.2020.111011
131. Y. Yulizar, E. Kusrini, D.O.B. Apriandanu, N. Nurdini, Datura metel L. leaves extract mediated CeO2 nanoparticles: synthesis, characterizations, and degradation activity of DPPH radical. Surf. Interfaces. **19**, 100437 (2020). https://doi.org/10.1016/j.surfin.2020.100437
132. K. Lalhminghlui, G.C. Jagetia, Evaluation of the free-radical scavenging and antioxidant activities of Chilauni, Schima Wallichii Korth in vitro. Future Sci. OA **4**(2), Fso272 (2018). https://doi.org/10.4155/fsoa-2017-0086
133. M.M. Rahman, M.B. Islam, M. Biswas, A.H.M. Khurshid Alam, In vitro antioxidant and free radical scavenging activity of different parts of Tabebuia pallida growing in Bangladesh. BMC Res. Notes. **8**(1), 621 (2015). https://doi.org/10.1186/s13104-015-1618-6
134. E.A. Adebayo, J.B. Ibikunle, A.M. Oke, A. Lateef, M.A. Azeez, A.O. Oluwatoyin et al., Antimicrobial and antioxidant activity of silver, gold and silver-gold alloy nanoparticles phytosynthesized using extract of Opuntia ficus-indica. Rev. Adv. Mater. Sci. **58**(1), 313–326 (2019)
135. A. Abida, M.H. Almutairi, N. Mushtaq, M. Ahmed, N. Sher, F. Fozia et al., Revolutionizing nanotechnology with Filago desertorum extracts: biogenic synthesis of silver nanoparticles exhibiting potent antioxidant and antibacterial activities. ACS Omega. **8**(38), 35140–35151 (2023). https://doi.org/10.1021/acsomega.3c04373
136. M.-H. Moosavy, de la M. Guardia, A. Mokhtarzadeh, S.A. Khatibi, N. Hosseinzadeh, N. Hajipour, Green synthesis, characterization, and biological evaluation of gold and silver nanoparticles using Mentha spicata essential oil. Sci. Rep. **13**(1), 7230 (2023). https://doi.org/10.1038/s41598-023-33632-y
137. G.J. Kontoghiorghes, C.N. Kontoghiorghe, Iron and chelation in Biochemistry and Medicine: New approaches to Controlling Iron Metabolism and Treating Related diseases. Cells. **9**(6) (2020). https://doi.org/10.3390/cells9061456
138. N.E. Rainey, A. Moustapha, A. Saric, G. Nicolas, F. Sureau, P.X. Petit, Iron chelation by curcumin suppresses both curcumin-induced autophagy and cell death together with iron overload neoplastic transformation. Cell. Death Discov. **5**, 150 (2019). https://doi.org/10.1038/s41420-019-0234-y
139. R. Sudan, M. Bhagat, S. Gupta, J. Singh, A. Koul, Iron (FeII) chelation, ferric reducing antioxidant power, and immune modulating potential of Arisaema Jacquemontii (Himalayan Cobra Lily). Biomed. Res. Int. **2014**, 179865 (2014). https://doi.org/10.1155/2014/179865
140. S. Nur, M. Aswad, R. Yulianti, F.J. Sami, A. Burhan, A. Fadri et al., Antioxidant activity profile of extract and fraction of kersen (Muntingia calabura L.) fruits prepared by different methods. IOP Conference Series: Earth and Environmental Science. 2022;976(1):012066. https://doi.org/10.1088/1755-1315/976/1/012066
141. S. Tavakoli, M.A. Ebrahimzadeh, F. Sameni, P. Biparva, H. Mohammadi, A. Ziar et al., Excess iron ion reduction in a thalassemia model using silver nanoparticles modified by the tannin fraction of Myrtus communis extact. Nanomed. Res. J. **5**(4), 355–363 (2020). https://doi.org/10.22034/nmrj.2020.04.007
142. M. Alavi, N. Karimi, Characterization, antibacterial, total antioxidant, scavenging, reducing power and ion chelating activities of green synthesized silver, copper and titanium dioxide nanoparticles using Artemisia haussknechtii leaf extract. Artif. Cells Nanomed. Biotechnol. **46**(8), 2066–2081 (2018). https://doi.org/10.1080/21691401.2017.1408121
143. G. Mahendran, B.D. Ranjitha Kumari, Biological activities of silver nanoparticles from Nothapodytes Nimmoniana (Graham) Mabb. Fruit extracts. Food Sci. Hum. Wellness. **5**(4), 207–218 (2016). https://doi.org/10.1016/j.fshw.2016.10.001
144. N. Suganthy, V. Sri Ramkumar, A. Pugazhendhi, G. Benelli, G. Archunan, Biogenic synthesis of gold nanoparticles from Terminalia arjuna bark extract: assessment of safety aspects and neuroprotective potential via antioxidant, anticholinesterase, and antiamyloidogenic effects. Environ. Sci. Pollut. Res. **25**(11), 10418–10433 (2018). https://doi.org/10.1007/s11356-017-9789-4
145. S. Bhakya, S. Muthukrishnan, M. Sukumaran, M. Muthukumar, Biogenic synthesis of silver nanoparticles and their antioxidant and antibacterial activity. Appl. Nanosci. **6**(5), 755–766 (2016). https://doi.org/10.1007/s13204-015-0473-z
146. N. Kanipandian, S. Kannan, R. Ramesh, P. Subramanian, R. Thirumurugan, Characterization, antioxidant and cytotoxicity evaluation of green synthesized silver nanoparticles using Cleistanthus collinus extract as surface modifier. Mater. Res. Bull. **49**, 494–502 (2014). https://doi.org/10.1016/j.materresbull.2013.09.016
147. S. Ali, S. Sulaiman, A. Khan, M.R. Khan, R. Khan, Green synthesized silver nanoparticles (AgNPs) from parrotiopsis jacquemontiana (Decne) Rehder leaf extract and its biological activities.

Microsc. Res. Tech. **85**(1), 28–43 (2022). https://doi.org/10.1002/jemt.23882

148. R. Subramanian, P. Subbramaniyan, V. Raj, Antioxidant activity of the stem bark of Shorea roxburghii and its silver reducing power. SpringerPlus. **2**(1), 28 (2013). https://doi.org/10.1186/2193-1801-2-28
149. A. Muthuvel, K. Adavallan, K. Balamurugan, N. Krishnakumar, Biosynthesis of gold nanoparticles using Solanum nigrum leaf extract and screening their free radical scavenging and antibacterial properties. Biomed. Prev. Nutr. **4**(2), 325–332 (2014). https://doi.org/10.1016/j.bionut.2014.03.004
150. G. Sathishkumar, P.K. Jha, V.V. C, R. M, Cannonball fruit (Couroupita guianensis, Aubl.) Extract mediated synthesis of gold nanoparticles and evaluation of its antioxidant activity. J. Mol. Liq. **215**, 229–236 (2016). https://doi.org/10.1016/j.molliq.2015.12.043

Publisher's Note Springer Nature remains neutral with regard to jurisdictional claims in published maps and institutional affiliations.